# Mass Transfer Effect to Electrochemical Reduction of $CO_2$: Electrode, Electrocatalyst and Electrolyte

Shun Lu[a,1], Yucheng Wang[b,1], Hang Xiang[c], Hanhui Lei[b], Ben Bin Xu[b], Lei Xing[d], Eileen Hao Yu[cd*], Terence Xiaoteng Liu[b*]

a Chongqing Institute of Green and Intelligent Technology, Chinese Academy of Sciences, Chongqing 400714, China

b Faculty of Engineering and Environment, Northumbria University, Newcastle upon Tyne NE1 8ST, United Kingdom

c School of Engineering, Newcastle University, Newcastle Upon Tyne NE1 7RU, United Kingdom

d Department of Chemical Engineering, Loughborough University, Loughborough LE11 3TU, United Kingdom

Corresponding authors: Terence.liu@northumbria.ac.uk (T. Liu) and e.yu@lboro.ac.uk (E. Yu)

[1] These authors (S. Lu and Y. Wang) contributed equally to this work.

**Abstract:**

Electrochemical carbon dioxide reduction reaction ($eCO_2RR$) to value-added chemicals is considered as a promising strategy for $CO_2$ conversion with economic and environmental benefits. Recently, investigations in $eCO_2RR$ to produce chemicals as energy or chemical industrial feedstock has received much attention. The $eCO_2RR$ generally occurs at the interface between electrode/electrocatalyst and electrolyte including charge transfer, phase transformation and mass transport. One of key problems in the electrochemical reaction is mass transfer limitation owing to the gaseous property of $CO_2$ with low concentration on the surface of electrode/electrocatalyst. Several strategies were employed to improve mass transfer in the past years, including electrochemical reactors, electrodes, electrocatalysts and electrolytes, etc. which could low reaction barriers so adequately that reaction rates can be realized that are sufficient for $eCO_2RR$. This article comprehensively reviewed development related to mass transfer study of $CO_2$, including the mechanism of mass transfer of $CO_2$, and main factors (electrodes, electrocatalysts and electrolytes) on two-phase or multi-phase interface during $eCO_2RR$. The article is not aim at providing a comprehensive review of technical achievements towards $eCO_2RR$ technology, but rather to highlight electrode, catalyst, electrolyte, and other factors, which can understand the above components or factors' effects toward mass transfer investigations, to decouple mass transfer limitations and improve the performance of electrochemical $CO_2$ conversion. Furthermore, the challenges and perspectives for mass transfer to electrochemical $eCO_2RR$ are proposed.

***Keywords:*** electrochemically $CO_2$ reduction, mass transfer, electrode, electrocatalyst, electrolyte

## 1. Introduction

Many nations in the world have launched actions for carbon emission reduction over the past decades, it is further urged by the 'net zero' target act and the 2021 United Nations climate change conference (COP26) that emerging technologies development of carbon capture and utilization are in high demand [1], containing direct carbon capture and storage [2, 3], artificial photosynthesis [4, 5], enhanced weathering [6, 7] and electrochemical $CO_2$ conversion [8], etc. Among them, electrochemical conversion of $CO_2$, also mostly referred as electrochemical $CO_2$ reduction reaction ($eCO_2RR$) is appealing because they operate with high reaction rates and excellent efficiencies under facile conditions, employ environmentally benign aqueous electrolytes, and easily combine with renewable sources (e.g. wind, solar, hydroelectric, etc.) [9, 10]. Another advantage of $eCO_2RR$ technology is that the conversion of $CO_2$ into value-added chemicals and fuels, is determined by the electrode, electrocatalyst, solvent, local pH, electrolyte, and $CO_2$ in-cell pressure, etc [10, 11]. One of the key limiting factors in $eCO_2RR$ is mass transfer dynamics of $CO_2$ to the cathode surface, such as the low solubility of $CO_2$ in the electrolyte, the supply of $CO_2$ to the porous electrode, pH value of electrolyte, and the properties of the electrocatalysts, even the electrolyzer design [12, 13]. Several solutions were also developed, e.g. gas diffusion electrode (GDE), which is a kind of electrically conductive composite coated on porous frameworks, has the merit of building stable and extended three-phase boundaries of gas-liquid-solid interface, shortening the gas diffusion path and improving mass transfer, and thus has been extensively applied in the $eCO_2RR$ [14, 15]. Additionally, the diffusion kinetics of $CO_2$ or protons at the interface of electrode/electrolyte has been identified as equally important to impact the $eCO_2RR$ performance. Given few reviews reporting on mass transfer effect on $eCO_2RR$, our attention is not to provide a complete review of the field but rather to highlight electrode, catalyst, electrolyte, and other factors, which can understand the above components or factors' effect toward mass transfer dynamics, further affect the performance of electrochemical conversion of $CO_2$.

The $eCO_2RR$ system cell structure can be summarized into two main categories, 1) two-chamber cell (2-C cell) and 2) GDE cell, as shown in **Fig. 1**. Both kinds of $CO_2$ cell structures have the same mechanism of $eCO_2RR$ in which water is oxidized to molecular oxygen at the anode, whereas $CO_2$ is reduced to carbon-based species at the cathode, and there is an ion exchange membrane placed between the anode and cathode in both $CO_2$ cells. In the cells, the undesired hydrogen evolution reaction (HER) is still competitive at the cathode during $eCO_2RR$ due to the presence of water [16-18]. For cathode reaction, $CO_2$ is an extremely stable molecule ($\Delta E$ = 532 kJ $mol^{-1}$, bond-dissociation energy at 298 K), therefore, external energy input is desired to drive the whole reaction. In general, the process of single-electron $CO_2$ reduction to $CO_2^{\cdot-}$ is -1.90 V vs. SHE (standard hydrogen electrode), leading the reaction difficult and unfavourable. Oppositely, proton-assisted electron transfer processes are more promising with different applied potentials in the range of -2.0 to 0.5 V vs. RHE (**Table 1**). **Table 1** proposed several typical products related with the $eCO_2RR$ and their equivalent standard reduction potentials ($E^0$). All mentioned potentials are referenced against the reversible hydrogen electrode (RHE). Here, the relationship between SHE and RHE is $E_{RHE} = E_{SHE} - 0.0592\ V \times pH$ (25 °C and 1 atm). The HER occurs at $E^0 = 0$ and can compete with $CO_2$ reduction at more negative potentials. Recent catalyst developments have focused on improving selectivity and controlling the

amount of co-evolved $H_2$ during $eCO_2RR$. However, the proton-assisted reactions could produce a wide distribution of carbon-based species, this result is associated with electrocatalysts, applied potentials, electrolytes, etc. Those factors decrease the selectivity of the desired chemicals because of similar potentials applied in all the reaction pathways (**Table 1**). Mass transfer of $CO_2$ issue makes the situation becoming even worse in an aqueous electrolyte-based $CO_2$ cell. This is because of the intake of $CO_2$, $CO_2$ pressure inside the cell, a proton in aqueous electrolyte, and pH value can affect the formation of intermediates, $CO_{2^{\cdot}}$, further influence the reactivity and selectivity of $eCO_2RR$.

**Table 1** Standard reduction potentials ($E^0$) during $eCO_2RR$ with several products and reaction mechanisms.

| Product | Reaction | $E^0$/V (*vs.* RHE) |
|---|---|---|
| $CO_2^{\cdot-}$ | $CO_2 + e^- \rightarrow CO_2^{\cdot-}$ | -1.5 |
| $H_2$ | $2H^+ + 2e^- \rightarrow H_2$ | 0 (HER) |
| CO | $CO_2 + 2H^+ + 2e^- \rightarrow CO + H_2O$ | -0.11 |
| HCOOH | $CO_2 + 2H^+ \rightarrow HCOOH$ | -0.25 |
| HCHO | $CO_2 + 4H^+ + 4e^- \rightarrow HCHO + H_2O$ | -0.07 |
| $CH_3OH$ | $CO_2 + 6H^+ + 6e^- \rightarrow CH_3OH + H_2O$ | 0.02 |
| $CH_4$ | $CO_2 + 8H^+ + 8e^- \rightarrow CH_4 + 2H_2O$ | 0.17 |
| $C_2H_6$ | $CO_2 + 12H^+ + 12e^- \rightarrow C_2H_6 + 2H_2O$ | 0.06 |

In this article, we comprehensively summarized recent progress related to mass transportation of $CO_2$, including the mechanism of $CO_2$ mass transfer, and the main components (electrode, electrocatalyst and electrolyte) of mass transfer during $eCO_2RR$. The article is not aim at providing a comprehensive review of technical achievements towards $eCO_2RR$ technology, but rather to highlight electrode, catalyst, electrolyte, and other factors, which can understand the above components or factors' effects toward mass transfer investigations clearly, to decouple mass transfer limitations and improve the performance of electrochemical $CO_2$ conversion. Furthermore, the challenges and perspectives for mass transfer to electrochemical $eCO_2RR$ are also proposed.

## 2. Understanding of $CO_2$ Mass Transfer

Generally, the mass transfer of $CO_2$ during electrochemical $CO_2RR$ means $CO_2$ transport from its gas phase to the adjacent region of the reaction interface, which depends on the $CO_2$ supply method to some extent, is of great importance other than the pristine activity of electrocatalysts [19-21]. Notably, mass transfer of protons cannot be ignored for both $eCO_2RR$ and HER and affects the selectively consequently. As presented in **Fig. 1a**, "$CO_2$ purging into electrolyte" and **Fig. 1b** "$CO_2$ diffusion from gas diffusion electrode (GDE)", performed by a two-chamber (2C) cell and a GDE cell respectively, are the two main $CO_2$ supply methods applied in existed works field [22]. Song et al. [23] used liquid-phase and gas-phase systems to define and distinguish these two $CO_2$ supply methods in their paper. Promising reaction performance with high selective production of CO, formate, and $C_2$-$C_4$ hydrocarbons or

their oxygenates has been achieved by both two $CO_2$ supply methods [24-26], while the GDE system generally reached a high geometric current density [9, 27, 28]. For the further development of $CO_2$ reduction, it is imperative to study the $CO_2$ mass transfer process and the corresponding influence factors based on these two popular systems.

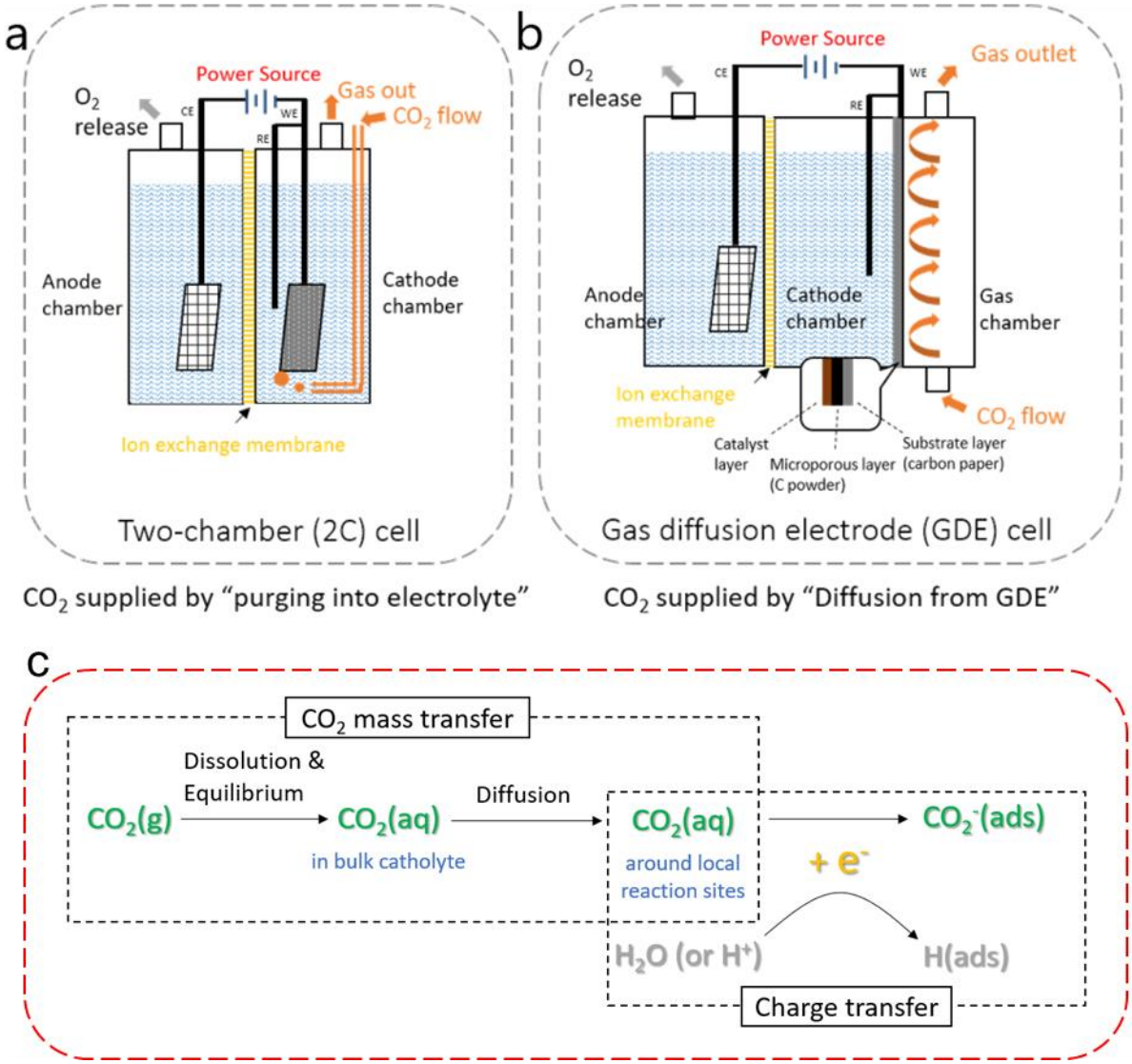


**Figure 1.** (a-b) Illustration of the two general electrolyzers: (a) 2C-cell and (b) GDE-cell to achieve the $CO_2$ supply method of "purging into electrolyte" and "diffusion from GDE" respectively. (c) Mass transfer of $CO_2$ and competitive charge transfer in aqueous $eCO_2RR$ system applying the $CO_2$ supply method of "purging into electrolyte". [29] Copyright 2019, Elsevier.

### *2.1 $CO_2$ Purging into Electrolyte*

The pre-bubbling of $CO_2$ is necessary before reaction to reach the saturation solubility of $CO_2$ into the catholyte. It has been widely accepted that the real reactant in the $eCO_2RR$ system is the dissolved $CO_2$ (written as $CO_2$ (aq) or $H_2CO_3$*), rather than ionic $HCO_3^-$ and $CO_3^{2-}$ [18, 30, 31]. As presented in **Fig. 1c**, the process of $CO_2$ mass transfer

in aqueous medium is composed of two major steps: Step 1. $CO_2$ gas dissolution and equilibrium to produce the reactant $CO_2$ (aq), Step 2. $CO_2$ (aq) diffusion from bulk catholyte to local reaction sites. The rate of each step at different pH conditions and the corresponding influence factors are summarised in **Table 2**.

As shown in **Table 2**, Step 1 primarily consists of a physical mass transfer process as illustrated in **Eq. 1**, and chemical reaction (3) or (5) (depending on pH of electrolyte), positively providing and negatively consuming the reactant $CO_2$ (aq) respectively. The rate of $CO_2$ (aq) generation via the physical mass transfer process was described in **Eq. 2**, which is a function of the gas/liquid mass transfer coefficient $k_{G/L}$, specific gas/liquid surface area $a$, $CO_2$ partial pressure $p_{CO2}$, and the equilibrium constant $K_0$. The $eCO_2RR$ performances could be developed by optimizing this process. Hori et al. [79] found the partial current density of CO production on the gold electrode presented a linearly rising trend with the $CO_2$ partial pressure $p_{CO2}$ within the range from 0.25 to 1.0 atm. In order to enhance the specific gas/liquid surface area $a$, Peter et al. [11] applied a glass frit bubbler to produce microbubbles with less than 0.2 mm radius. The $CO_2$ microbubbles contributed to a higher hydrocarbon/$H_2$ ratio in the products of $eCO_2RR$, in comparison with bigger $CO_2$ bubbles (~0.5 mm radius) provided by a capillary tube bubbler. The equilibrium constant $K_0$ is a temperature-dependent constant, decreased with higher temperature. Thus, the $R_{MT}$ is inversely correlated with the temperature, which is the reason for a declined $CO_2$ solubility in aqueous solution with increasing temperature.

However, chemical reaction (3) or (5) consumes the formed $CO_2$ (aq) immediately. When pH in the solution is lower than 8, reaction (3) dominates the whole chemical step which is a sluggish step with forward reaction rate ($k_{+0}=3.0\times10^{-2}$ $s^{-1}$) much smaller than the backward reaction rate ($k_{-0}=23.7$ $s^{-1}$). Given this phenomenon, several studies used acidic catholyte to ease the $CO_2$ (aq) consuming process. When pH of electrolyte is over 10, reaction (5) dominates the whole chemical process which is a very fast step with the forward reaction rate ($k_{+1}=8.5\times10^{3}$ $s^{-1}$) much bigger than the backward reaction rate ($k_{-1}=2.3\times10^{-4}$ $s^{-1}$). Therefore, when purging $CO_2$ gas into alkaline electrolyte, the bulk solution turned to be neutral quickly. Overall, according to the two dynamic processes of $CO_2$ (aq) providing and consumption simultaneously, how much $CO_2$ (aq) (or $H_2CO_3$*) could be balanced eventually is one of the most important principles of catholyte selection. Zhong and co-workers calculated the $H_2CO_3$* equilibrium concentrations after $CO_2$ bubbling into some commonly used catholyte, among which, $KHCO_3$ solution is selected to be the optimal catholyte since it can balance higher concentration of $H_2CO_3$* [18]. 0.1 M, 0.5 M and 1.5 M $KHCO_3$ solutions balanced 33 mM, 37 mM and 45 mM $H_2CO_3$* respectively after $CO_2$ bubbling, which means $KHCO_3$ with higher concentration has slightly more dissolved $CO_2$ reactant.

**Table 2** $CO_2$ mass transfer steps and the corresponding rates

| | Positive process | Negative process | Rate of the process |
|---|---|---|---|
| Step 1<br>Dissolution and Equilibrium | Physical mass transfer:<br>$CO_2(g) + H_2O\ (l) \overset{K_0}{\leftrightarrow} CO_2(aq) + H_2O\ (l) = H_2CO_3^*$ (1) | | $R_{MT} = k_{G/L} a p_{CO2} K_0$ (2)<br>$R_{MT}$: mass transfer rate (M $s^{-1}$)<br>$k_{G/L}$: mass transfer coefficient (m $s^{-1}$),<br>$a$: specific gas/liquid surface area ($m^2$ $m^{-3}$),<br>$p_{CO2}$: $CO_2$ partial pressure(kPa)<br>$K_0$: equilibrium constant, $= 1 \times 10^{18} T^{-8.7051}$ (M $kPa^{-1}$) |
| | | Chemical reaction:<br>$CO_2(aq) + H_2O(l) \underset{k_{-0}}{\overset{k_{+0}}{\rightleftharpoons}} H_2CO_3 \rightleftharpoons H^+ + HCO_3^-$ (3)<br>pH < 8[32] | $-\frac{d[CO_2(aq)]}{t} = k_{+0} h_L \varepsilon [CO_2(aq)]$ (4)<br>$k_{+0}$: rate constant, =$3\times10^{-2}$ ($s^{-1}$)<br>$h_L$: liquid hold-up<br>$\varepsilon$: voidage of 3D cathode<br>$CO_2(aq)$: concentration of dissolved $CO_2$ in bulk electrolyte (M) |
| | | pH > 10<br>$CO_2(aq) + OH^- \underset{k_{-1}}{\overset{k_{+1}}{\rightleftharpoons}} HCO_3^-$ (5) | $-\frac{d[CO_2(aq)]}{t} = k_{+1} h_L \varepsilon [CO_2(aq)][OH^-]$ (6)<br>$k_{+1}$: rate constant, =$8.5\times10^3$ ($s^{-1}$) |
| | | 8 < pH < 10, (3) and (5) both take place | $-\frac{d[CO_2(aq)]}{t} = (k_{+0} + k_{+1}[OH^-]) h_L \varepsilon [CO_2(aq)]$ (7) |
| Step 2<br>Diffusion | $CO_2$ (aq) diffusion from the bulk electrolyte to local active sites | | Fick's Second Law<br>$\frac{\partial C}{\partial t} = -D \frac{\partial C^2}{\partial x^2}$ (8)<br>$C$: concentration of $CO_2$ (aq) (M)<br>$x$: diffusion distance (m)<br>$D$: diffusion coefficient of $CO_2$ (aq) in water ($m^2$ $s^{-1}$)<br>$t$: time (s) |

Unfortunately, Step 2 will further reduce the concentration of $CO_2$ (aq) by the diffusion pathway and time, which is a physical diffusion process following Fick's Second Law [12]. The diffusion coefficient *D* is a complex function of the intrinsic physical properties of electrolytes and environmental conditions. Owing to the smaller liquid viscosity of more dilute solution under higher temperatures, $D_{CO2}$ in an aqueous solution is positively correlated to temperature but negatively correlated to the salt concentration [33]. Thus, $KHCO_3$ solution with a higher concentration stronger constrains $CO_2$ (aq) diffusion in this step, even though it can balance more $CO_2$ (aq) after Step 1. Moreover, under the reduction potential, the diffusion of $CO_2$ (aq) adjacent to the double layer is more complex due to the adsorption of cations. Joaquin et al. found that although the alkali metal cations wouldn't be reduced under the potential of $eCO_2RR$, they would be hydrated and absorbed around the outer Helmholtz layer of cathode and create a dipole electric field (1 V $Å^{-1}$), whose stabilization decreases the energy for $^*CO_2$ adsorption [34]. Accordingly, the higher salt concentration of the catholyte doesn't facilitate $CO_2$ (aq) diffusion in this step because of the lower diffusion coefficient and larger coverage of cations around the reaction sites. This diffusion problem along with the high concentrated catholyte was observed by Hori et al. [30] and Xiang et al. [29] that with the $CO_2$ supply method of "purging into electrolyte", the ratio of carbonaceous products/$H_2$ from $eCO_2RR$ decreased with the increasing catholyte salt concentration. When applying "purging into electrolyte" method to supply $CO_2$, mass transfer of $CO_2$ is mainly constrained by the low solubility and inefficient diffusion from the bulk electrolyte to the local reaction sites, resulting in incomparable competitiveness of $eCO_2RR$ against HER and reduced current efficiency of carbonaceous products.

### *2.2 Diffusion from Gas Diffusion Electrode (GDE)*

Conventionally, researchers are focusing on the development of catalysts for higher reaction activity. However, once the catalysis activity has been enhanced, the low solubility of $CO_2$ can cause the low mass transfer problem and will be the rate-determine-step of the overall reaction system, which hind its reaction efficiency and cause low currently density. To solve the low solubility problem of $CO_2$, an increasing number of GDE-related works have been published in the past years for the sake of improving the mass transfer of $CO_2$, as $CO_2$ gas could be fed directly to the reaction sites with an efficient gas-liquid-solid three-phase boundary. This gas supply method has been applied in hydrogen-oxygen fuel cells for a long time [35], the direct gas adsorption has been accepted as the mass transfer mechanism of the gas reactants $H_2$ and $O_2$ [13, 36, 37]. Similarly, the reactant of $eCO_2RR$ by applying $CO_2$ "diffusion from GDE" was perceived to be gaseous $CO_2$ [38, 39] rather than the hydrated $CO_2$ (aq), which was already discussed in section **2.1**. Therefore, $CO_2$ gas could be directly adsorbed and activated by a less-restricted pathway without going through catholyte media, as illustrated in **Eq. 9**.

$$CO_2(g) \xrightarrow{e^-} CO_2^-(ads) \qquad (9)$$

The most outstanding achievement of applying GDE in $eCO_2RR$ is the remarkable current density (*j*) which is normally over hundreds of mA $cm^{-2}$, bring the industrial potential to this currently bench-scale reaction [23]. In fact, it was found that electrolyte played the predominant role in the high current density achievement rather than the effect of $CO_2$ supply way [29]. Strong alkali with a high concentration of $OH^-$ enabled low resistance in both the cell

internal and charge transfer was certificated to be the optimum aqueous electrolyte for $eCO_2RR$ [40]. The use of strong alkaline media as the catholyte could also prevent the competing HER appeared.

$CO_2$ mass transfer enhanced with a big step when transiting the $CO_2$ supply method from "purging into electrolyte" to "diffusion from GDE". As far as we know, apart from the development of electrode material/catalyst, there seem to have few reported works about further enhancing the $CO_2$ mass transfer in the GDE system in a macro view like cell configuration and reaction conditions. Only a few studies were carried out on the effect of cell pressure in $eCO_2RR$ process [41-44]. Gabardo et al. [41] studied the pressurization effects on $eCO_2RR$ selectivity and efficiency in the GDE cell, and the faradaic efficiency (FE) of CO was enhanced by about 40% when rising the cell pressure from 1 to 7 atm. The reason for the selectivity shift was assumed to be the increased $CO_2$ surface coverage.

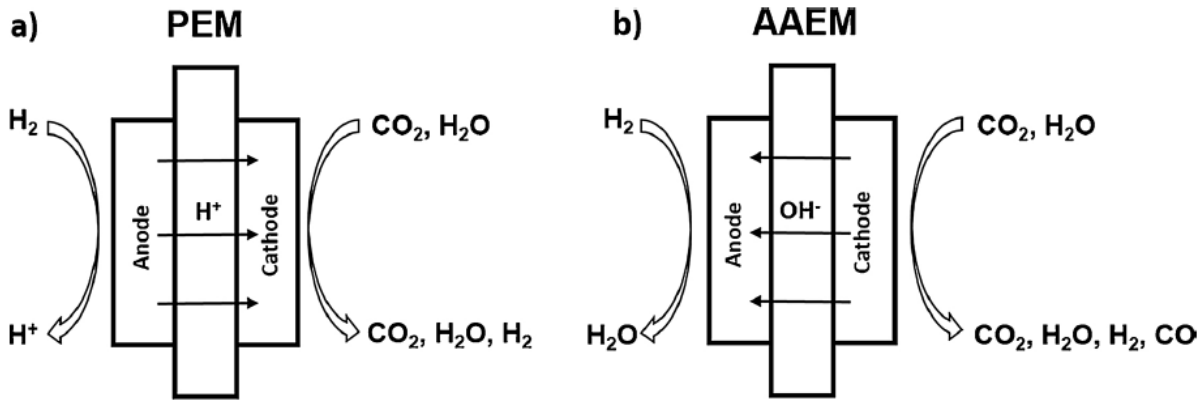


**Figure 2.** Scheme of the $eCO_2RR$ reactor with the MEA configuration. The difference in ion transfer of using (a) proton exchange membrane (PEM), and (b) alkaline anion exchange membrane (AAEM). [45] Copyright 2018, Elsevier.

It is worth mentioning that the GDE system applying liquid catholyte commonly suffers the flooding problem. Poor reaction stability of fewer than 10 hours was observed accordingly, since the hydrophobic layers within GDE can be degraded during electrolysis, especially in alkaline media[20]. The infiltration of liquid catholyte into the $CO_2$ gas phase alters the $CO_2$ supply method from "diffusion from GDE" back to "purging into electrolyte", $CO_2$ mass transfer is reduced by this degradation. A novel electrode architecture was then delivered by Dinh et al. [40], to create an abrupt interface with graphite/carbon nanoparticles/Cu catalyst/PTFE layer to overcome the liquid electrolyte flooding issue. The reaction could be maintained with 70% FE towards $C_2H_4$ for 150 hours. Wang et al. [46] reported a scaffolding structured catalyst layer in a GDE system, which enhanced the internal porosity and the hydrophobicity of GDE and raise the FE of CO up to 93.2%. Apart from constructing a robust GDE to avoid flooding, some studies abandoned the liquid electrolyte and adopted the polymer electrolyte membrane (PEM) to fabricate a membrane electrode assembly (MEA) in a compressed reactor [47]. Protons can be supplied by vapour co-streamed with the $CO_2$ gas or ion migration from the anodic side via a PEM as illustrated in **Fig. 2** [45]. Lee et al. [38] applied the Sn-GDE (cathode), Nafion membrane, and Pt-GDE (anode) to fabricate the MEA for formate production from $eCO_2RR$, a high FE about 90% was maintained for 50 hours. Kutz et al. [48] developed a robust

membrane with using imidazolium-functionalized stylene and vinylbenzyl chloride polymer for e$CO_2$RR with an MEA configuration, showing remarkable durability of around 6 months for producing CO with 90% FE and 50 mA $cm^{-2}$ of current density [48].

Overall, the liquid-phase system of applying "purging into electrolyte" method to supply $CO_2$ is simple and handy to construct but constrains $CO_2$ mass transfer by the liquid electrolyte media. Applying "diffusion from GDE" in the gas-phase system is a promising transit to perform a high-performance mass transfer and developed current efficiency towards $CO_2$ reduction, but the flooding problem will lead to poor durability which can be alleviated by adopting a polymer electrolyte membrane. The development of $CO_2$ mass transfer from a macro view has been approached by improving the reactor configuration and optimising the reaction conditions, contributing to higher $CO_2$ coverage around the cathode. The further $CO_2$ mass transfer from the cathode adjacency to the reaction sites more relies on the electrode material or catalyst, and electrolyte, which will be discussed in the next section.

## 3. The Effect of Components for Mass Transfer of $CO_2$

The process of $CO_2$ mass transfer can be associated with many factors, including but not limit to types of electrodes, electrolyte concentration, pH of electrolyte, applied catalyst, membrane, flow rate of $CO_2$, etc., which could greatly influence the result. Herein we pick three factors to clarify how theses component effect on mass transfer of $CO_2$. For the overall reaction, electrode delivers the electrons and $CO_2$ (in gas diffusion electrode), the electrolyte transfers the proton and $CO_2$ (aq, in H-type cell), and the reaction take place on the catalyst surface active sites. Good balance of three factors could optimise the performance, otherwise it can be the constraint which limit the overall reaction.

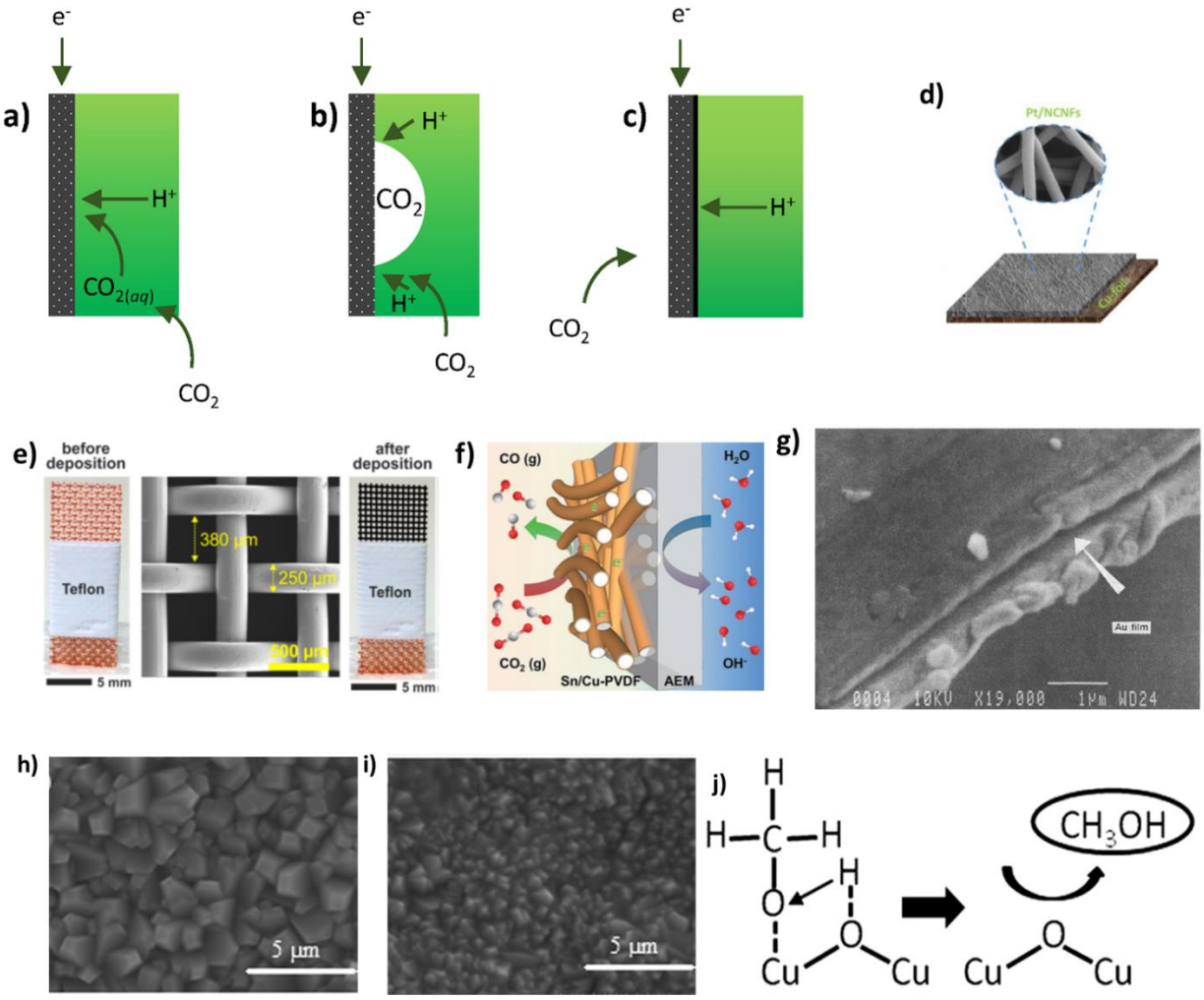


**Figure 3.** (a) $CO_2$ transfer in aqueous phase by dissolving in electrolyte. (b) purged $CO_2$ bubble block the catalyst surface by H-cell (c) $CO_2$ transfer through gas diffusion layer (GDL) by GDE type cell.[49] Copyright 2021, Wiley-VCH. Common $eCO_2RR$ electrodes (d) foil electrode. [50] Copyright 2018, Elsevier, (e) mesh electrode. Reprinted with permission from [19] Copyright 2017, American Chemical Society, and (f) GDE. [51] Copyright 2019, Wiley-VCH. (g) SEM of the thin layer photoresist edge of a polymide/gold/photoresist image with 1 µm thickness of gold film.[52] Copyright 1991, Elsevier. Electrodeposited cuprous oxide film (h) before reaction and (i) after reaction. (j) Hydrogenation of methoxy adsorbates at $Cu_2O$ {111} surfaces. [53] Copyright 2011, The Electrochemical Society.

### *3.1 Electrode*

In the $eCO_2RR$ process, the function of the electrode includes catalysts substrate, mass transfer, and GDE of $CO_2$, which are the crucial parts of $eCO_2RR$. From the viewpoint of the electrode, the interface of electrode/electrolyte is the place where loading with electrocatalyst, providing conductive support for most electrochemical reactions. The coming reactants including electron, proton, and $CO_2$ meet in triple interphase (gas, liquid, and solid phase) boundary, and then take reaction on the active sites of catalysts. Wang et al. [49] revealed the interphases using different electrode types, wherein sheet-like electrode or other bulk electrodes, the common

supplying method of $CO_2$ is to 'bubbling into electrolyte' and diffuse to electrode surface. The two-phase interphase can be generated as shown in **Fig. 3a**, where the $CO_{2(aq)}$ with $H_{+(aq)}$) and electrons can meet on the liquid(electrolyte)-solid (catalyst) interphase, and take the reaction. This configuration will lack $CO_2$ due to its low solubility as illustrated in **Section. 2**. In **Fig. 3b**, the $CO_2$ bubble may stick to the catalyst surface and form a triple-phase at the edge of the bubble, however, within the gas bubble, the reaction will be stopped by the absence of electrolyte with $H^+$. In **Fig. 3c**, $CO_2$ is supplied from the gas phase and diffused through the electrode. This configuration can be realized by porous electrodes. However, hydrophobicity is the key point to preventing the electrolyte pass through. Metal mesh with bad hydrophobicity in this application will cause electrolyte permeation and loss the function. In comparison, the gas diffusion electrode has a porous structure and good water resistance, which is the desired material for three face interphase configurations.

The transport of proton and $CO_2$ is controlled by diffusion, and diffusion is the movement of chemical species from high to low concentration. The movement rate of chemicals by diffusion can be predicted theoretically. Fick's Law demonstrates that the diffusional flux is proportional to the concentration gradient $\partial C/\partial x$ of the diffusing solute, as shown in **Eq. 10** [54].

$$J_o = -D_O\left(\frac{\partial c_O}{\partial x}\right) \qquad (10)$$

where $J_o$ is the diffusional flux, the constant $D_o$ is the diffusion coefficient (diffusivity), and the negative sign means the concentration gradient from high to low.

To achieve the diffusion of reactants in $eCO_2RR$ process, the catalysts' surface area, active sites on the catalyst, transportation of electrons, protons and $CO_2$ molecules should be well considered in the reaction system [55]. Based on the existed publications, the rate of mass transport can affect or even dominate the overall reduction reaction. **Eq. 11** presents below presents the relation between current and several factors which can affect the mass transfer of $CO_2$.

$$i_c = -nFAk_{re}[o] \qquad (11)$$

Where $i$ is the reaction current, $A$ is the electrode area, $k_{re}$ is the rate constant and [o] is the concentration of reactant.

If the constant is large enough which means any reactants can be immediately converted to products when they close to the electrode interface, then the determined part will be the concentration of reaction will be the overall rate determined aspect [54]. Perry et al. [55] illustrated two distinct limitations for mass-transport on electrodes. The first limitation is the diffusion of reactants gathered onto the electrode, and the second limitation is about the non-uniform current distributions caused by ohmic loss on electrodes. Therefore, the improvement of mass transfer on electrode assembly becomes an effective solution for $eCO_2RR$ commercialization. Recently, researchers focused on catalysts innovations and developed types of catalysts with considerable efficiencies and selectivity. However, few of these catalysts were measured under commercially relevant current densities (ca. 200 mA $cm^{-2}$) owing to mass transport limitations under conventional optimized conditions [56]. Moreover, 2-C cells are widely used for electrolysis, and the long-distance between electrodes requires much stronger current densities to overcome the mass

transport issues [57]. To solve the transportation problem, novel types of electrodes are considered to be thin layers with more active points [20]. Given this point, various electrodes with functional structure (**Fig. 3d-f**) were developed by researchers. The species of electrodes can be classified as catalysis macro-structure, including sheet (*e.g.*, foil and film), mesh, foam, and metal powder-gas diffusion layer (GDL).

### *3.1.1 Sheet-like electrode*

The sheet-type electrode is one kind of working electrodes for $eCO_2RR$. A two-dimensional surface provides sufficient surface area where the reaction takes place and these electrodes are normally assembled in a fully aqueous phase, which is for 2-C and GDE cell [53, 58-61]. In this case, $CO_2$ is required to dissolve into the catholyte to realize the mass transfer of $CO_2$. Sheet-type electrodes can be classified into pure foil, porous foil and nanoparticles supported foil, indicating the treatment of electrodes realizes the foil with better surface area [62-64]. Pure metal foil electrodes normally appeared in early-stage research. For example, Hori et al. discovered that methane and ethylene can be produced at Cu electrode in 0.5 M $KHCO_3$, the current density was detected at 5 mA $cm^{-2}$, with FE of $CH_4$ was about 65% at 0 °C, and $C_2H_4$ with 20% at 40 °C [65, 66]. Kim. et al. [62] reported that reduction of $CO_2$ to $CH_4$ on Cu foil electrode under room temperature. They prepared Cu polycrystalline sheets in 0.5 M $KHCO_3$ under -0.50 V vs. SCE under ambient conditions, achieving the transition of $CO_2$ to $CH_4$ with a current density of 17 mA $cm^{-2}$. Researchers have developed that the $eCO_2RR$ are limited by lacking mass transport and a larger surface area could provide more active sites which can contribute larger current. Seddon et al. [52] employed gold thin film spun onto polymer sheets with thickness of 1 and 4 μm, as shown in **Fig. 3g**. By enhancing diffusional transport to a finite electrode surface under microscopic size, the current has been significantly increased.

Oxidation treatment of metal is another method for electrodes preparation. Metal oxides provide chemical functionality, which can stabilize the incipient negative charge on $CO_2$ and mediate the electron transfer [60]. Le et al. [53] reported that cuprous oxide thin film has obtained 43% FE of $CH_3OH$ with 43 μmol $cm^{-2}$ $h^{-1}$, as shown in **Fig. 3i-j**. When HCO species form, carbon atom continues proton and electron transfer reactions to form $H_3CO^*{}_3CO^*$ species adsorbates for $CH_4$ formation. In the case of the presence of cuprous oxide, it will benefit the ability of $H^+$ species coordinated with surface bound oxygen to form $CH_3OH$. Chen et al. [60] employed tin oxide thin film for $CO_2$ reduction, and illustrated that the rate determine step is the reversible transfer of a single electron to $CO_2$, then form $CO_2^{\cdot-}$[67], the current density can be increased by improvement of $CO_2$ and ion mass transport and achieved the nearly 100% FE with CO and HCOOH using $Sn/SnO_x$ foil. Le et al. [53] also reported a 40% FE of methanol by electrodeposited cuprous oxide films.

Nano porous film is another type of sheet electrode in $CO_2$ reduction [68-70], and the porous structure is normally realized by the dealloying method. Jia et al. [68] indicated an alloy-dealloy method to manufacture nanoporous film in order to get high surface material, which is using the electrodeposition method to obtain several types of nanoporous metal films. The process introduced electrodeposition of Zn on metal film including Cu, Ag and Au, then thermo-treat the surface and immersed into the etching solution to get nanoporous surface. In this case, a porous structure can both provide high surface area, and be directly formed on the electrode surface, in which the electronic transport will be much faster. However, the transport of $H^+$ promotes the water splitting behaviour, which

competes with $CO_2$ reduction. Chen et al. [69] reported a highly porous gold film with increased pH of electrolyte, which could prohibit hydrogen evolution reaction. They also developed a porous structure of Au porous structure on Ag film, which could promote ion transfer. They have compared the different thickness of Au porous layer, and the observed current density was increased by the thickness of Au layer, as shown in **Fig. 4**.

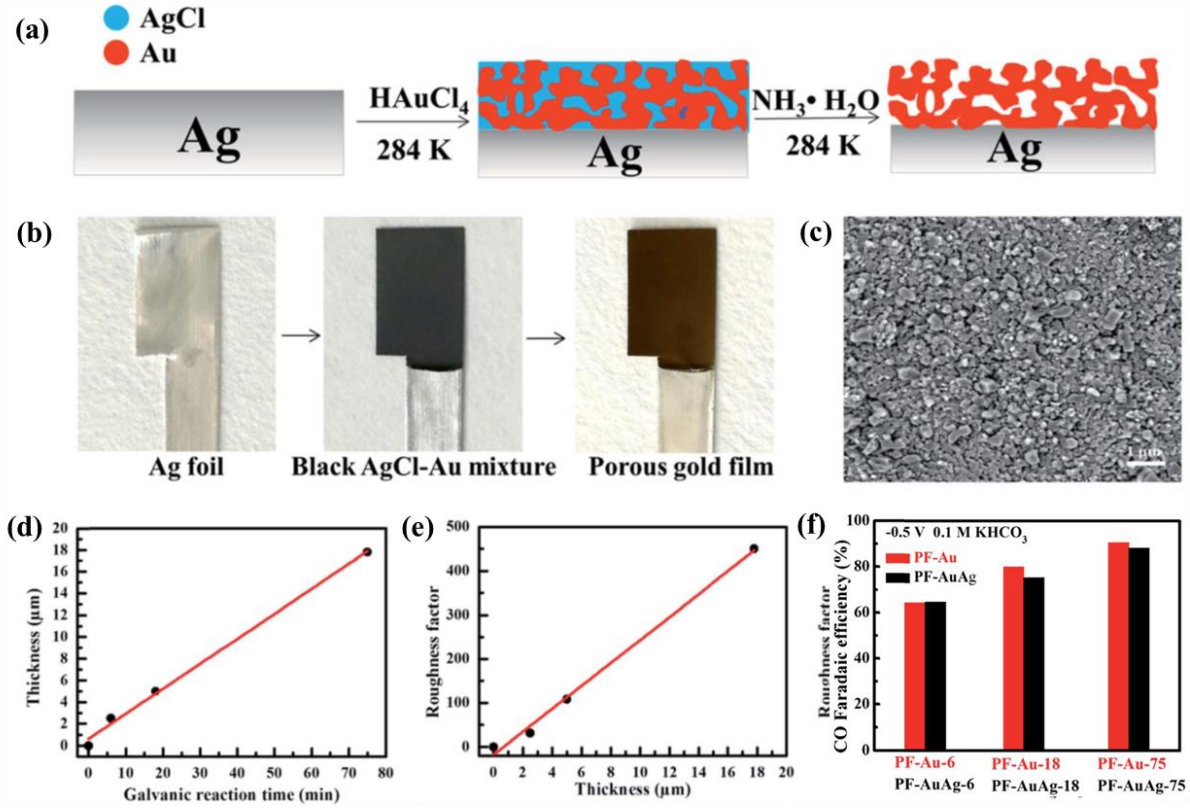


**Figure 4.** (a) Schematic design of key fabrications in designing porous gold films. (b) Physical images of the porous gold film lying on the Ag foil. (c) SEM image of the porous AgCl-Au precursor. (d) Film thickness as a function of galvanic reaction times of the silver substrate and $HAuCl_4$. (e) The plots between the roughness and film thickness of the PF-Au samples, and the surface roughness of the pre-treated Ag plate is 1. (f) $FE_{CO}$ faradaic at -0.5 V. [69] Copyright 2017, The Royal Society of Chemistry.

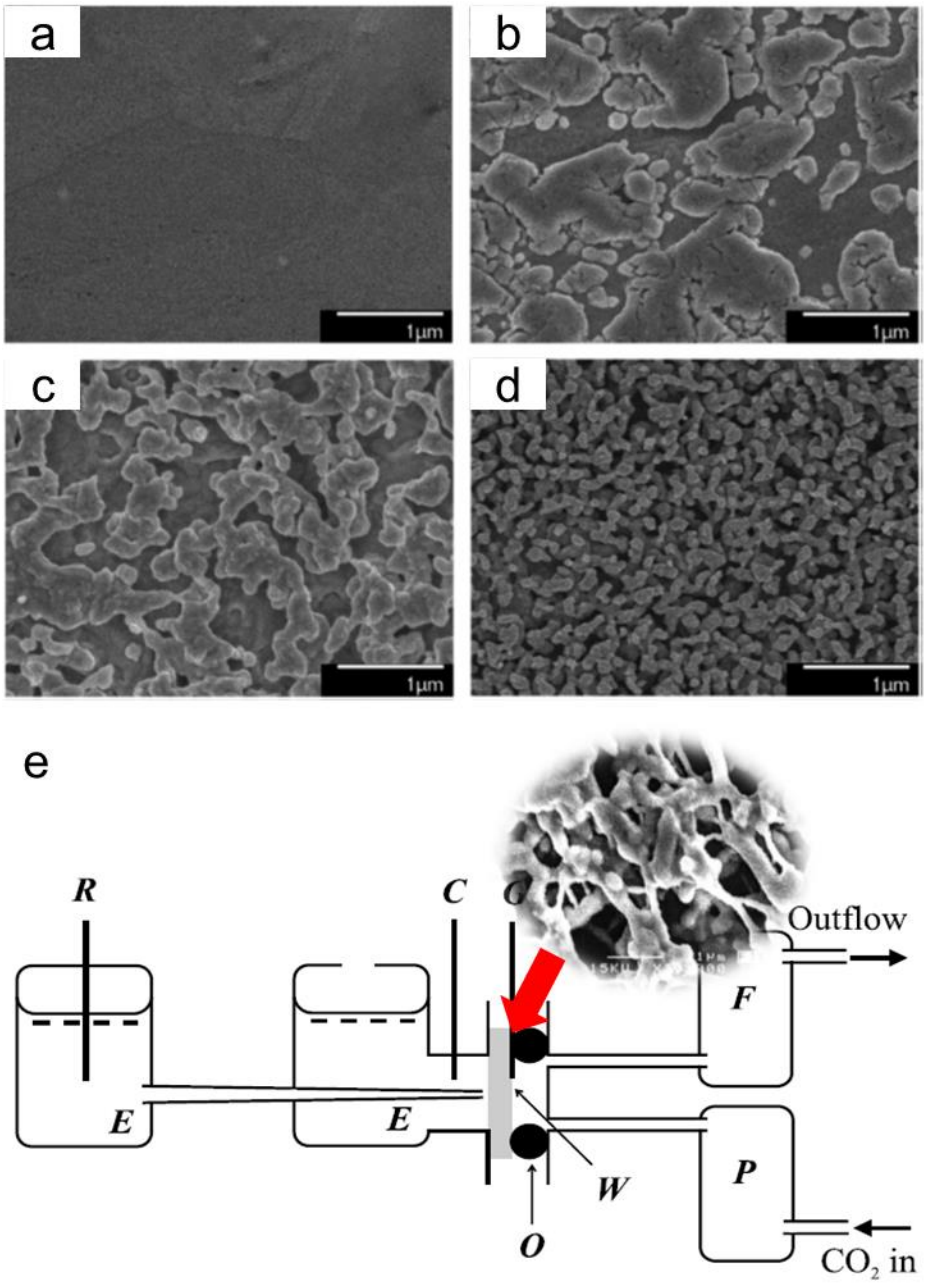


**Figure 5.** SEM images of (a) polished copper foil, (b) np30, (c) np60, and (d) np120. Reprinted with permission from [70] Copyright 2017, American Chemical Society. (e) Schematic diagram of the electrochemical cell. R, saturated calomel reference electrode; C, Pt wire coil counter electrode; E, 500 mM $KHCO_3$ electrolyte; W, working electrode; G, gold leaf contact to the working electrode; O, ring seal; P, inlet pressure gauge; F, outlet pressure gauge and flow meter, inset: scanning tunnelling microscope image of the surface of the porous Au layer. [71] Copyright 2002, Elsevier.

Peng et al. [70] obtained a porous Cu foil by alloying-dealloying method, with 35% FE of ethylene in 0.1 M $KHCO_3$ under -1.3 V vs. RHE. They used electrodeposition treatment of zinc onto polished copper foil and then obtained a nanoporous surface structure by chemical dealloying method. XRD pattern indicated the identity of the material surface and SEM image shows its nanoporous structure (**Fig. 5**). By controlling zinc deposition time, the

distribution of products was analysed, and the overall FE of hydrocarbons is increasing with electrodeposition time. The ethylene and formic acid can be obtained under -1.1 to -1.3 V vs. RHE with an FE of 35%. The author indicated that the complicated skeleton structure and porous structure contribute large surface area. Stevens et. al. reported a porous Au film that presents good properties to convert $CO_2$ to CO with FE of 75% under -1.2 V vs. SCE in aqueous $KHCO_3$ using an original GDE type cell (**Fig. 5e**) [71]. The porous Au film was used to separate the liquid and gas phases, which improves the mass transfer of $CO_2$.

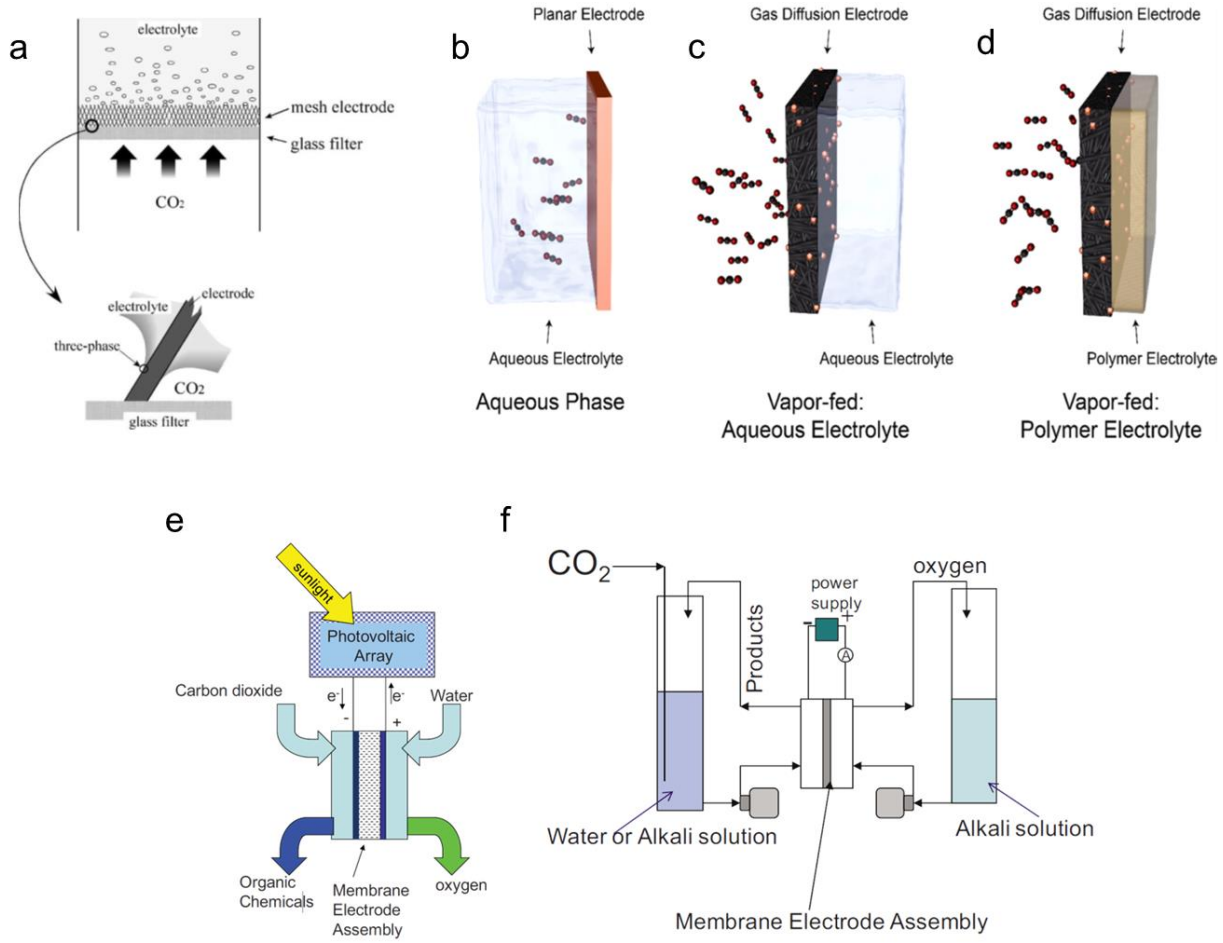


**Figure 6.** (a) Schematic representation of three-phase (gas/liquid/solution) interface. [72] Copyright 2004, Elsevier. Different electrochemical $eCO_2RR$ reactor schemes. (b) Aqueous-phase $eCO_2RR$, where $CO_2$ is first solubilized in an aqueous electrolyte and then reduced at a catalyst surface. Vapor-fed $eCO_2RR$ employing a (c) aqueous or (d) polymer electrolyte. Reprinted with permission from [20] Copyright 2018, American Chemical Society. (e) Polymer membrane cell configuration for the electrochemical reduction of carbon dioxide, (f) Schematic of the experimental arrangement to produce organic products from carbon dioxide using a membrane cell. [73] Copyright 2011, The Electrochemical Society.

### *3.1.2 Meshes*

Compared with foil, metal mesh have a microporous structure, indicating its mesoporous structure can form more like channel compared with porous structured catalysts, which allow gas/electrolytes to across over, enhancing the surface area and have more chance to form gas ($CO^2$)-liquid(electrolyte, proton)-solid (catalyst) three-phase

interface (**Fig. 6a**) to complete the mass transfer of $CO_2$ in the three-phase interface [72, 74]. Ogura et al. developed a three-phased design with the assistance of the mesh structure [72, 75]. They established a vertical assembled cell and the $CO_2$ reduction has performed at the three-phase interface to avoid *in situ* reaction which causes the poisoning species after the beginning of electrolysis. $CO_2$ was recycled constantly in the device which enriched the $CO_2$ concentration on the interface that enhances the overall $CO_2$ reduction reaction. In their study, they used a CuBr modified on Cu-mesh for the working electrode, and the result indicates 90% of $CO_2$ conversion rate with 75% selectivity for $C_2H_4$. Similarly, Li et al. reported a continuous reactor using tinned-copper mesh as electrode, and supplied catholyte and $CO_2$ mixture cross through the as-mentioned electrode [74, 76].

Normally, the gas supply from one side of the mesh flows across the mesh and forms three-phase interface. This improves the mass transport with hollowed structure. The application of mesh type electrode for $CO_2$ reduction including normal mesh and surface modification on the mesh. In the early stage, researchers are more focused on the mesh's unique properties. Hirata et al. [77] reported an amalgamated-gold mesh electrode. DEMS (Differential Electrochemical Mass Spectroscopy) technique was selected, and Hg-Au was used as a working electrode that allows the gas to cross over, enhancing the performance of reduction from $CO_2$ to CO under -1.4 V vs. SCE. The three-phase interphase concept was emphasized by H. Yano [75, 78], which indicated that a triple interface can be realized by letting $CO_2$ gas blow across copper mesh constantly, performed three-phase (gas-liquid-solid, GLS) interface can extremely suppress the deposition of poisoning species behaviour and form long-term reaction. Recently, surface treatment for mesh electrodes is also received much attention. Hwang et al. [79] fabricated $Cu_2O$/CuO/CuS nanocomposites using pure copper mesh, this ternary electrocatalyst has 84% FE of formic acid during $eCO_2RR$. Rahaman et al. [19] illustrated that using electrodeposition of dendritic Cu on Cu mesh for catalysis properties enhancing. Results show high selectivity for formate and $C_2H_4$ at different potentials ($FE_{EtOH}$ = 13.0%, −1.0 V vs. RHE; $FE_{n\text{-}PrOH}$ = 13.1%, −0.9 V vs. RHE).

### *3.1.3 Gas Diffusion Electrodes*

Gas diffusion electrodes (GDEs) type electrodes have been first proposed in fuel cell application since 1967 [80]. Gas diffusion layer is normally involved in gas diffusion electrode assembly type cells for $eCO_2RR$, where GDE was initially introduced to enhance the gas mass transfer [81]. This concept is inspired by proton exchange membrane (PEM) fuel cell design, which is a porous material composed of carbon fibre or metal foams. In $eCO_2RR$ application, GDL are involved to applied a diffusion pathway which benefits the $CO_2$ transfer [29, 82], and catalyst layers coated on GDL as the electrode is a common way for the electrode assembly. In recent studies, Higgins et al. indicated that GDEs present excellent mass transport properties compared with conventional aqueous-phase $CO_2$ reaction [20, 56], which the poor solubility of $CO_2$ in aqueous electrodes problems can be solved. They supplied $CO_2$ to the cathode via vapour phase (**Fig. 6b-d**) is a solution for resolving the performance and solubility challenges. It also provides robust support for catalysts, and gas permeability, which prevent the electrode from being flooded by electrolyte and provides an electron transfer pathway [83]. It is typically hydrophobic, thus the surface and pores cannot be blocked by water molecules which may impede the gas transport to the catalyst layer [35], where the performance of GDE is determined by the effectivity of gas transmission of GDL [82].

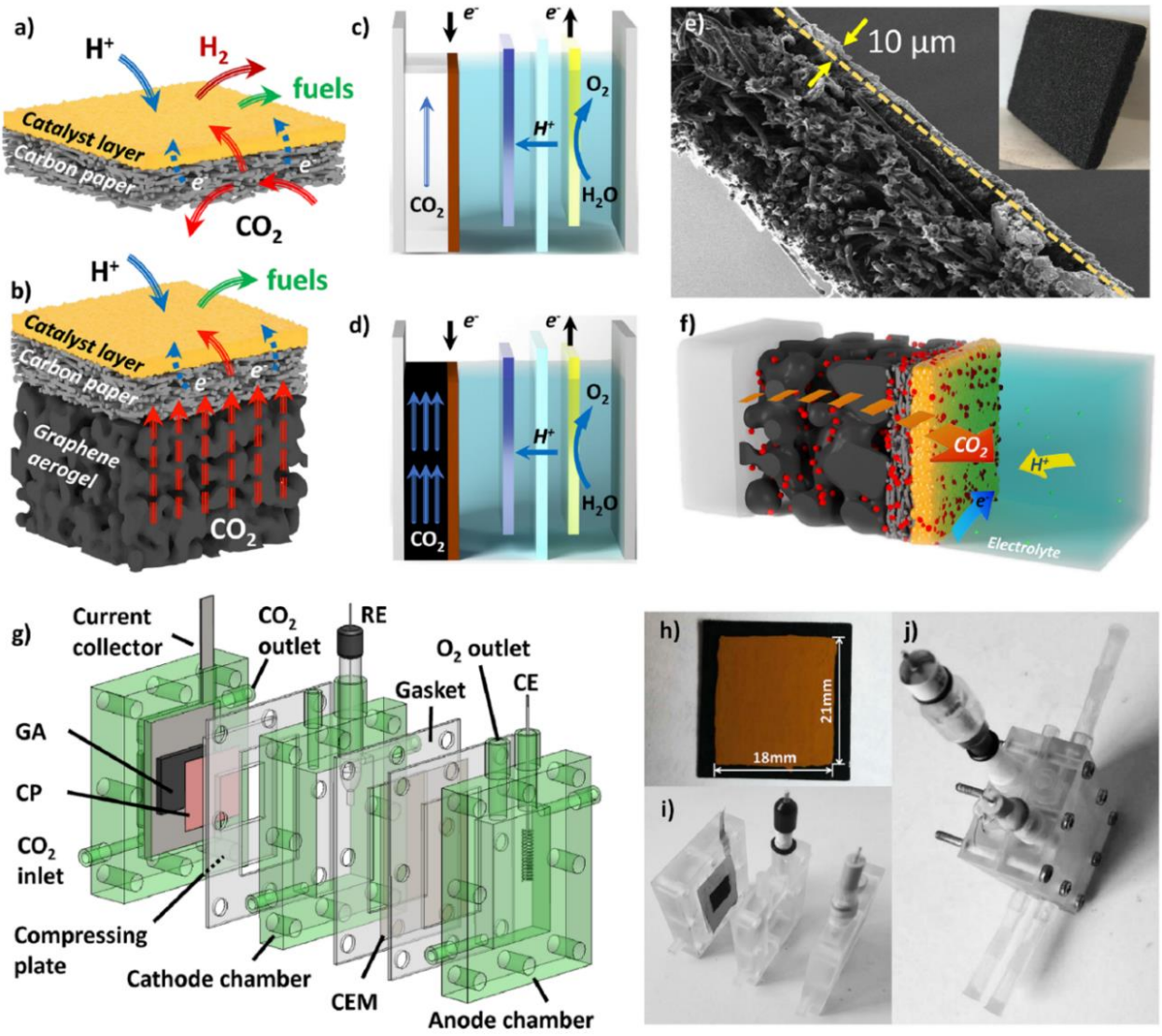


**Figure 7.** Schematic illustrations of design for (a) carbon paper (CP)-electrode, (b) graphene aerogel/carbon paper (GACP)-electrode; integrated design for (c) CP-cell and (d) GACP-cell, components arrangement from left to right are gas chamber (white: gas channel for CP-cell, black: GA for GACP-cell, respectively), catalyst coated carbon paper (brown), reference electrode (blue) in catholyte, ion exchange membrane (light blue), counter electrode (yellow) in anolyte; (e) cross-section view of the bilayer with catalyst layer and GA (insertion); (f) $CO_2$ mass transfer pathway, $CO_2$ transfer through GA (black), CP (grey) and catalyst layer (yellow); fabrication of GACP-cell with (g) multi-components, (h) top view of bilayer with coated catalyst, i) disassembled and j) assembled cells.[49] Copyright 2021, Wiley-VCH.

Compared with metal mesh, it allows $CO_2$ to flow across the GDE body and it is hydrophobic which means it can prevent the electrolyte from crossover and forming gas-electrolyte-catalysts three-phase interface. It is concluded to have two main electrode designs using GDE from the reported paper. One common electrode assembly design is called membrane electrode assembly (MEA), which is regarded to resolve the mass transfer issue in aqueous electrolytes. MEA design removed the electrolytes and minimize the ohmic overpotential by decreasing the distance between anode and cathode [84]. Narayanan et al. [73] reported a kind of MEA-type cell (**Fig. 6e-f**) with lead and indium and achieved the $FE_{HCOOH}$ of 90%, where they believe that the hydrogen evolution reaction (HER)

was suppressed by the catalysts where they have high overpotential for HER and absence of aqueous electrolytes on cathode part. Wang et al. [49] reported a hybrid carbon paper with graphene aerogel electrode for $eCO_2RR$, where the high porous and conductive graphene aerogel enhances the $CO_2$ mass transfer and charge transfer, and carbon paper plays a function of catalyst substrate, this combination which presents a great enhancement of $eCO_2RR$ performance, and has raised the $FE_{CO}$ to 94% (**Fig. 7**). Another electrode is that separates the cathode half-cell into two individual phases by using a catalyst on GDL to make a gas-liquid-solid phase interface. Compared with conventional H-type cell or 2-C cell, the separated design enhanced the gas transfer significantly by supplying $CO_2$ from the gas phase. It eliminates the $CO_2$ dissolving problem in electrolyte, simultaneously.

### 3.2 Electrocatalysts

Large number of various catalysts in micro- and nano-scale toward $eCO_2RR$ were investigated since 1980s. Before understanding the relationship between electrocatalysts and the mass transfer effect during $eCO_2RR$, it is necessary to understand and summarize the classification of various electrocatalysts. Early studies in $eCO_2RR$ focused primarily on metallic catalysts (monometallic, alloys, and multi-metallic), due to their ease of synthesis, high stability, and simple morphology, making them suitable for fundamental $eCO_2RR$ studies. For instance, copper-based electrocatalysts received much attention owing to they can produce a range of useful chemicals ($C_1$-$C_4$ chemicals) with high FE. Therefore, a classification was early built based on the primary $CO_2$ reduction products, as shown in **Fig. 8**. With the extension of electrocatalysts, most existing $eCO_2RR$ catalysts can be divided into several groups with different classifications. In this section, all electrocatalysts for $eCO_2RR$ will be divided into 0-3D materials in regard to the dimensional structure. Generally, $CO_2$ will form into $^*CO$ intermediate species during the $CO_2$ transportation, then $^*CO$ will interact with $^*H$ or another $^*CO$ to produce $^*CHO$/C-C species on the interface between $CO_2$ and electrocatalyst. For example, 3D materials with more corner/edge sites and even porous structure [85], which can also adsorb $CO_2$ in a two-phase or three-phase system, further improve the electrocatalytic performance of $CO_2$ conversion. Additionally, catalysts' structural properties including crystal planes, surface area and size, etc. will also affect the mass transfer of $CO_2$ during $eCO_2RR$.

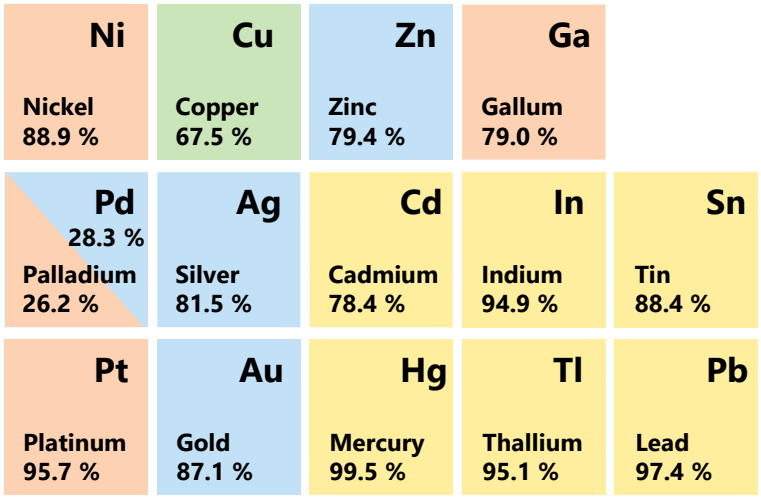

**Figure 8.** Classification of various metal depending on formation of major products during $eCO_2RR$, periodic table and FE of major products from experimental data by Hori. [30] $H_2$ (red), CO (blue), formate (yellow), hydrocarbon (green). Notably, the production distribution from $CO_2$ depends strongly upon the electrolytes employed. Copyright 1989, The Royal Society of Chemistry.

### *3.2.1 Catalysts' Dimensional Structure*

**0D structure** – Quantum dots (QDs) are typical zero-dimensional materials. For example, carbon quantum dots (CQDs) are attractive as a valuable element of photo/electro-catalysts due to their large number of exposed active sites and excellent electron transfer ability [86-88]. Moreover, the surface of CQD can be easily modified by several functionalized groups (e.g. $-NH_2$, -COOH), which can improve the $CO_2$ adsorption performance due to molecules interaction [86]. In addition, CQDs could be adopted to enhance the catalytic performance of $eCO_2RR$ due to the exposed active sites. Recently, N-doped graphene QDs (NGQDs) were selected as catalysts for $eCO_2RR$, NGQDs with high catalytic performance for $eCO_2RR$ with high current density at -0.75 V vs. RHE were reported [9]. As presented in **Fig. 9a**, NGQDs with a large portion of nitrogen atom doped defects at the edges were exfoliated [9]. More active sites were created during the doping of nitrogen atoms. It can be seen that $C_2H_4$ is the main product with a maximum FE of 90% in the range of applied potential from -0.75 to -1.0 V vs. RHE in **Fig. 9b**. Authors also studied the potential mechanisms governing the total process for NGQDs by performing first-principles simulations (**Fig. 9c-e**) [89]. In their study, they found that the insertion of N atoms into the edges of GQDs promotes the mass transfer with $^*$COOH, effectively enhancing the conversion of $CO_2$ to CO. Benefiting from the edge and defect effects and quantum confinement, QDs modified on substrates can promote the mass transfer of electroactive species and further enhance the $eCO_2RR$ performance through their synergistic effects [90]. This design (QDs/X, X refers substrates) also could promote the low-dimensional catalysts for efficient $eCO_2RR$.

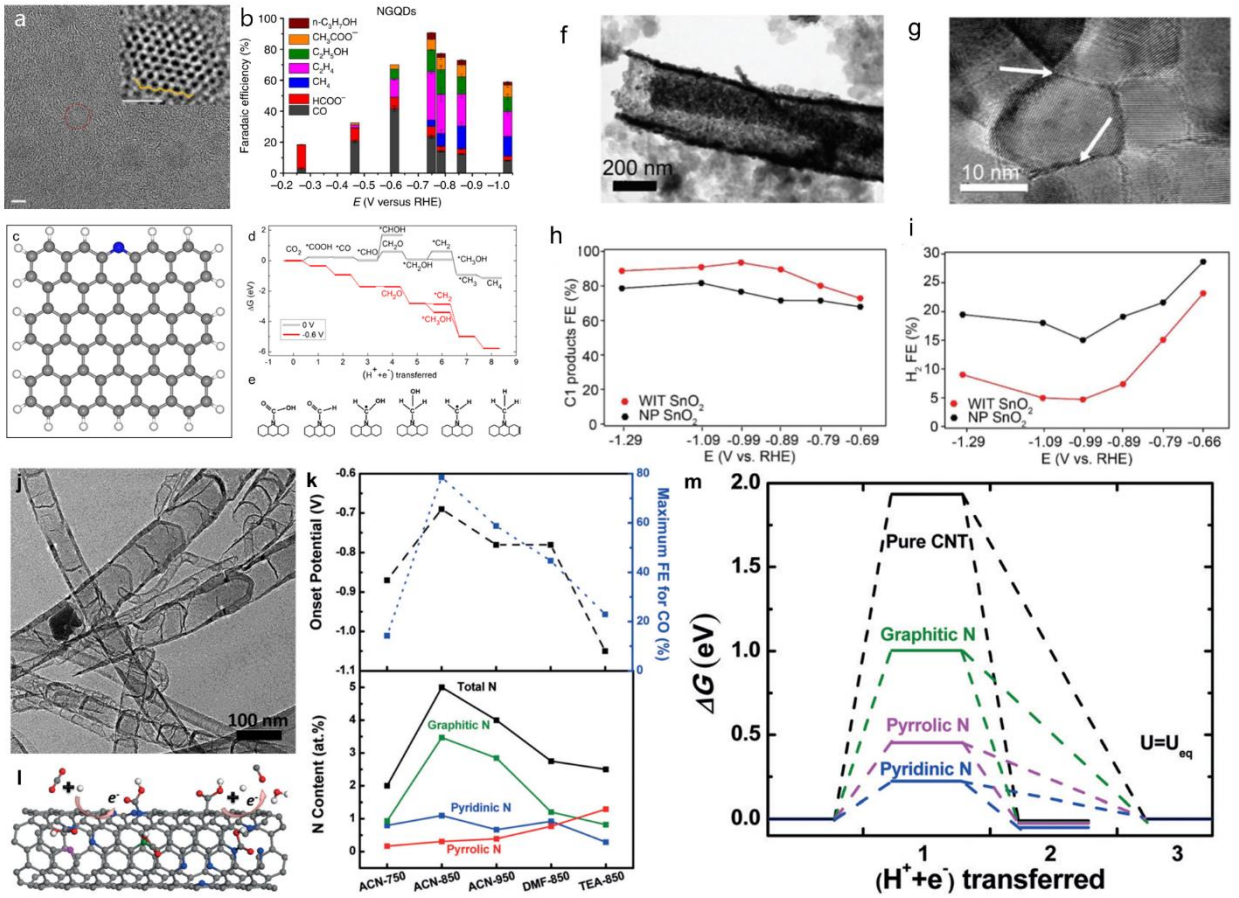


**Figure 9.** (a) High-resolution TEM image of NGQDs (scale, 2 nm). Inset: a single NGQD containing zigzag edges as circled (b) FEs of CO, $CH_4$, $C_2H_4$, $HCOO^-$, $C_2H_5OH$, $CH_3COO^-$ and n-$C_3H_7OH$ at various applied cathodic potential for NGQDs in the electrocatalytic activity of carbon nanostructures towards $CO_2$ reduction. [9] Copyright 2016, Nature Publishing Group. (c) Structural models and unit cells of NGQDs, Gray, blue, and white spheres represent carbon, nitrogen, and hydrogen atoms, respectively. (d) Energy pathways for electrochemical reduction of $CO_2$ to $CH_3OH$ and $CH_4$ at 0 V (black) and -0.6 V (red). (e) Schematic for selected intermediate states, including $^*COOH$, $^*CHO$, $^*CHOH$, $^*CH_2OH$, $^*CH_2$, and $^*CH_3$ adsorbed on NGQDs. Reprinted with permission from [89] Copyright 2017, American Chemical Society. (f-g) HRTEM image of the WIT $SnO_2$ after reduction, (h-i) FE of $C_1$ products and $H_2$ for the WIT $SnO_2$ electrode and the NP $SnO_2$ electrode. [91] Copyright 2018, Wiley-VCH. (j) TEM image of NCNTs, (k) the onset potential and maximum FE for CO formation as a function of N content in the synthesized NCNTs, (l) Schematic illustrating CO formation on the NCNTs and (m) free-energy diagram at equilibrium potential for $CO_2$ reduction on different N defects, including pyridinic, pyrrolic, and graphitic N in comparison to pristine CNTs. C, O, and H atoms are represented by grey, red, and white spheres, while pyridinic, pyrrolic, and graphitic N defects are shown using blue, pink, and green spheres, respectively. [92] Copyright 2015, Wiley-VCH.

**1D structure** – One dimensional (1D) nanomaterials, such as nanotubes and nanowires etc. provide a high active surface area have been employed in electrochemical reactions as catalysts in past years [93]. Owing to the enhanced contact with the electrolyte, 1D structure can accelerate the mass and charge transfer at the three-phase boundaries. Li et al. [91] demonstrated 1D $SnO_2$ with wire-in-tube (WIT) structure as an electrocatalyst for $CO_2$RR to $C_1$ products in $CO_2$ saturated $KHCO_3$ electrolyte (**Fig. 9f-g**). it shows a higher FE of $C_1$ products (>90%) than commercial $SnO_2$ nanoparticles at a wide applied potential range from −0.89 to −1.29 V vs. RHE, thus substantially suppressing HER (**Fig. 9h-i**). To explore possible boosted mechanisms for 1D WIT $SnO_2$, HRTEM and BET

characterizations were employed, it can be found a density of grain boundaries (GBs) during the calcining process via HRTEM observation (**Fig. 9g**). The BET results show that 1D WIT $SnO_2$ has larger surface area that that of NP $SnO_2$. This feature provides more active surface sites for $^{*}CO_2^{\bullet-}$ absorption, which facilitates the mass transfer of $eCO_2RR$. In addition, recent investigations have indicated GBs within the nanopores could generate high activity for $CO_2$ reduction through enhancing the adsorbate-metal bonding strengths thus stabilizing catalytically active surfaces, as for GBs analysis would be discussed in the following section.

It was found that nitrogen-doped carbon nanofibers (NCNFs) exhibited approximately 13-fold higher current density than Ag electrocatalyst under a selective reduction of $CO_2$ to CO [94]. Coupling with X-ray photoelectron spectroscopy and activity characterizations, the authors proposed the high reactivity and excellent durability of the NCNFs for the $eCO_2RR$ is ascribed to the charged carbon atoms because of N-doping inducing the re-distribution of the charge and spin density on NCNFs. Zhou et al. [95] discovered that nitrogen-doped carbon nanotubes (NCNTs) is a promising catalyst for $eCO_2RR$ conversion to CO with FE of 80%. Before being applied in $eCO_2RR$, NCNTs have received much attention as 1D nanostructured electrocatalysts in oxygen reduction reaction (ORR) and oxygen evolution reaction (OER) due to their unique electronic and geometric features [96]. NCNTs have also been employed for $CO_2$ reduction to formate using polyethyleimine as a co-catalyst, stabilizing the $^{*}CO_2^{\bullet-}$ intermediate [92]. In their earlier work, NCNTs were prepared with various surface structures and nitrogen contents by choosing different precursors (ACN: acetonitrile, DMF: dimethlyformamide and TEA: triethylamine) and controlling the growth temperature (**Fig. 9j**). It is found that the electrochemical performance of NCNTs was determined by the nature of N-defects and defect density in **Fig. 9k**. NCNTs-ACN-850 (NCNTs were obtained from the ACN which provides N source under 850 ℃) had the lowest overpotential (ca. -0.18 V) and maximum selectivity (ca. 80% FE) with the highest catalytic activity, owing to the highest pyridinic N (ca. 1.1 at%) and graphitic N (ca. 3.5 at%) content. Additionally, with the assistance of DFT investigations, $COOH^{*}$ tends to bind to the adjacent pyridinic-like N sites, rather than the pyrrolic N site during the $eCO_2RR$. Thereby, pyrrolic N defects seem to have little or no impact on $eCO_2RR$ activity, which is congruent with previous experimental observations. (**Fig. 9l-m**).

**2D structure** – 2D materials or layered materials, such as graphene [97], transition-metal dichalcogenides (TMDs) [98] and layered double hydroxides (LDHs) [99], etc., could transfer electrons even through the covalent bond network of metallic or nonmetallic constituents. 2D metallic materials are promising electrocatalysts for $eCO_2RR$, first studied theoretically by Kim at el. [100] as shown in **Fig. 10a-b**. A numerical study showed $E_{CO2ER}$ of 2D covalent metals using the reported computational procedure including the entropic contribution and solvation effect [101]. $H_2$ production is the major side reaction competing with $CO_2$ reduction in an aqueous circumstances, which should be hindered to reach high FE. The authors also obtained that the existence of strong scaling relationship between the COOH binding affinity and H binding affinity limits high selectivity toward $CO_2$ reduction. There is a linear correlation between $\Delta E_b^{COOH}$ and $\Delta E_b^{1/2H2}$, as shown in **Fig. 10b** ($\Delta E_b^{1/2H2}$ is the H binding energy defined using $1/2H_2(g)$ as a reference state), like existing transition metals. $\Delta E_b^{COOH}$ could be adjusted to increase for enhanced $CO_2$ reduction catalytic activity, which concomitantly increases the H binding affinity elevating the HER performance in most cases. Therefore, this is an important strategy for material optimization to overcome the

intrinsic limitations of metals or metallic alloys, improving $CO_2$ reduction with high performance from the above calculations.

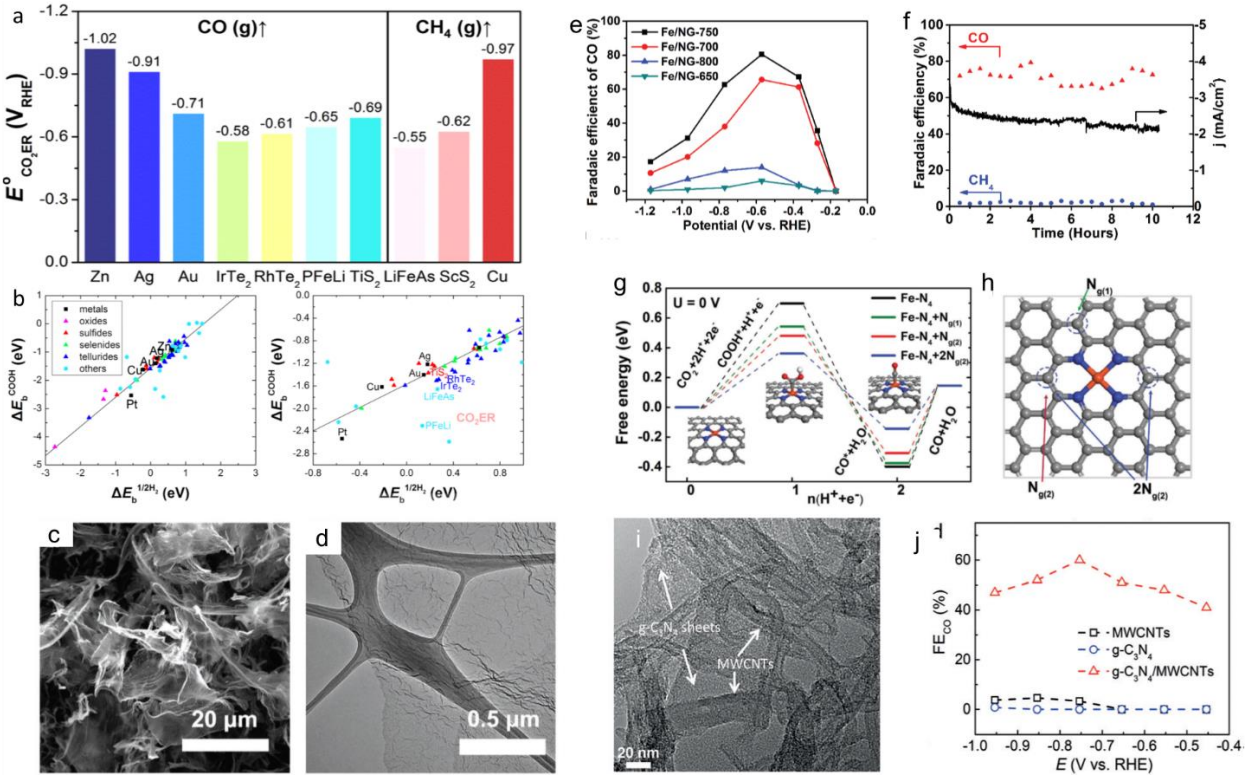


**Figure 10.** High-throughput catalyst screening of 2D covalent metals for $eCO_2RR$: using density functional binding free energies, theoretical reduction potentials of $CO_2$ (vs. RHE) into CO (left) or $CH_4$ (right) are calculated, (b) Mutual correlation between the $\Delta E^{COOH}$ and $\Delta E^{H}$ on the catalyst. Both 2D covalent metals and conventional transition metals show a relatively significant correlation. Reprinted with permission from [101]. Copyright 2016, American Chemical Society. (c) SEM image, (d) TEM image of Fe/NG-750 catalyst. (e) Potential dependent FE of CO for $eCO_2RR$ on Fe/NG catalysts prepared at different processed temperatures (0.1 M $KHCO_3$) (f) Chronoamperometric curves of stability test with Fe/NG-750 at −0.60 V versus RHE in the $CO_2$-saturated 0.1 M $KHCO_3$ solution. Theoretical calculations and proposed mechanism on the N-coordinated Fe catalytic site, (g) Free energy diagram for $eCO_2RR$ to CO on Fe-$N_4$ moieties embedded on graphene sheets. (h) Top view of the optimized structures for Fe-$N_4$ moieties embedded on graphene layer and potential N-substitution. [102] Copyright 2018, Wiley-VCH. (i) TEM image of the g-$C_3N_4$/MWCNT composite, (j) Dependence of FE of CO on applied potential during constant potential electrolysis of $CO_2$ obtained with pristine MWCNTs, pristine g-$C_3N_4$ and the g-$C_3N_4$/MWCNT composite coated carbon fibre papers, respectively. [103] Copyright 2016, Wiley-VCH.

Graphene-based materials have been widely utilized as metal-free electrocatalysts for $eCO_2RR$ application due to their extremely large surface area, mechanical stability and flexibility, and good electrical conductivity. The heteroatom-doped (e.g., B, N, and S etc.) graphene has displayed extraordinary $eCO_2RR$ performance. For example, Tour and co-workers reported an atomic Fe distributed on N-doped graphene (Fe/NG, **Fig. 10c-d**) was prepared as an efficient catalyst for the electrochemical reduction of $CO_2$ to CO [102]. In their bulk electrocatalysis, Fe/NG has a low reduction overpotential (0.3 V vs. RHE) with high FE up to 80% (**Fig. 10d**) and remained stable after the $eCO_2RR$ without any significant degradation (**Fig. 10e**). Based on DFT investigations [32, 104], the adsorption of $CO_2$ molecule primarily arises on the Fe catalytic site with concerted protonation and electron transfer, accounting

for the establishment of $COOH^*$, as Fe-$N_4$-COOH formed, it can endure further proton-electron transfer reduction to for a $CO^*$ adduct (**Fig. 10f**). Herein, the rate limiting step is the formation of $COOH^*$ species via protonation. The authors found that the N-doping on graphene improves the catalytic activity of the Fe-$N_4$ moieties by lowering the energy barrier of $COOH^*$ formation, as well as promoting the CO* desorption step according to the free energy diagram (**Fig. 10g-h**). It is concluded that the highly e$CO_2$RR performance of $CO_2$ conversion to CO could be ascribed to the synergetic effect of the Fe-$N_4$ moieties and N-doping on the graphene surface.

Graphitic carbon nitride (g-$C_3N_4$) is another group of metal-free 2D materials. The carbon species in g-$C_3N_4$ display high affinity to oxygen-bound intermediates ($^*OCH_x$, $^*O$, and $^*OH$) in the reaction routes toward deeply reduced products, e.g., methane. Furthermore, the electronic properties of g-$C_3N_4$ can be effectively tuned by metal and metal-free carbon materials and therefore provide improved electrocatalytic performance on the hybrid catalysts [103, 105]. For example, Amal et al. [103] demonstrated a g-$C_3N_4$/MWCNT composite (**Fig. 10i-j**) as a highly selective and stable electrocatalyst for $CO_2$ reduction to CO, in which the strongly formed covalent C-N bonds could become active sites to enhance e$CO_2$RR performance, combining the excellent electrical conductivity of MWCNT enables various electrons to rapidly reach the active C-N sites, giving rise to a FE of 60% of and remarkable durability over 50 h. These hybrid composites based on g-$C_3N_4$ have shown their promising e$CO_2$RR performance owing to their highly exposed active sites on the large surface of electrocatalysts with a high turnover number (TON), which means more $CO_2$ can contact those active sites easily, in other words, mass transfer was enhanced during this process. Combined with the enhanced mass transfer, improved electrical conductivity, and tunable electron transfer, the performance of $CO_2$ was also promoted synergistically.

**3D structure** – Most metal-organic framework (MOF) compounds can be considered nanoscale three-dimensional structured catalysts. MOFs combine the favorable characteristics of both heterogeneous and homogeneous catalysts [106, 107]. Developing MOFs and their derivatives as electrocatalysts are regarded as an efficient approach to reticulate catalytic molecular units into a porous structure in which active sites are maximized and both charge and mass transportation could be simultaneously balanced by tuning their porous structure [108, 109]. In addition, MOFs were also proven as efficient catalysts for e$CO_2$RR due to their 3D structure enabling $CO_2$ capture [110]. The mechanism of $CO_2$ capture is that $CO_2$ can be captured and separated when its molecular structure coordinates with the unsaturated metal sites in the MOF structure owing to the very small kinetic diameter of $CO_2$ (0.33 nm). For example, the $CO_2$ trapping capacity of Mg-MOF-74 was reported up to 8.9%, and 87% of trapped $CO_2$ could be released at room temperature, indicating capture capacity of this kind of MOF is controllable [111]. This strategy can solve a problem well that e$CO_2$RR was limited by the low $CO_2$ solubility, in some cases, shortening the gas diffusion process, keeping $CO_2$-saturated on the surface of the electrocatalyst, so that increasing the mass transfer in the special two-phase between $CO_2$ and catalyst layer, further improving $CO_2$ conversion efficiency. Such effect is further confirmed by Zhang et al. [112] who introduced $Cu_3(BTC)_2$ (BTC, Benzene-1,3,5-tricarboxylic acid) which is a kind of MOF that has demonstrated its $CO_2$ adsorption capacity can achieve 5 mmol $g^{-1}$ as $CO_2$ capture agent based on GDE (**Fig. 11a**). In this study, authors confirmed the $CO_2$ capture ability of the prepared $Cu_3(BTC)_2$ via $N_2$ adsorption-desorption at 77K, then the FE of $CH_4$ on Gu-MOF/GDE are 2-3 times

higher than that of the bare GDE under negative potentials in the range of 7.5%-10% (Cu-MOF weight ratio), as presented in **Fig. 11b**. The authors also believed the active sites in GDE-CuMOF-10 are not evidently blocked by Cu-MOF and implied the almost unaffected catalytic properties of Cu-MOF on the formation pathway of $CH_4$. Dong and co-workers also utilized the same principle to design Fe-porphyrin-based MOF (PCN-222(Fe)) for electrochemical reduction of $CO_2$ to CO [113]. In this study, the authors reported that the composite catalyst PCN-222(Fe)/C (mass ratio = 1:2) was prepared by a simple dip-coating process, it exhibited high $eCO_2RR$ performance with 494 mV overpotential (j = 1.2 mA $cm^{-2}$) and maximum 91% $FE_{CO}$ in a $CO_2$-saturated 0.5 M $KHCO_3$ aqueous solution, achieving a TOF (turnover frequency) of 0.012 $s^{-1}$ due to the combination of the intrinsic activity of porphyrin molecule, and the promising $CO_2$ adsorption ability endowed by the conserved porosity, as well as the high conductivity of carbon black. 3D MOF electrocatalysts have several advantages over other inorganic catalysts: (i) the reticular framework and the pore properties could be regulated and functionalized by the functionalized ligands or the secondary units which further increase active sites and specific surface area, promoting $CO_2$ of mass transfer between catalyst and carbon black, therefore optimize the reactivity and selectivity for $eCO_2RR$, (ii) the promising $CO_2$ adsorption ability of some MOFs is beneficial in $eCO_2RR$ since the reduction kinetics are closely related to the $CO_2$ concentration [112, 113].

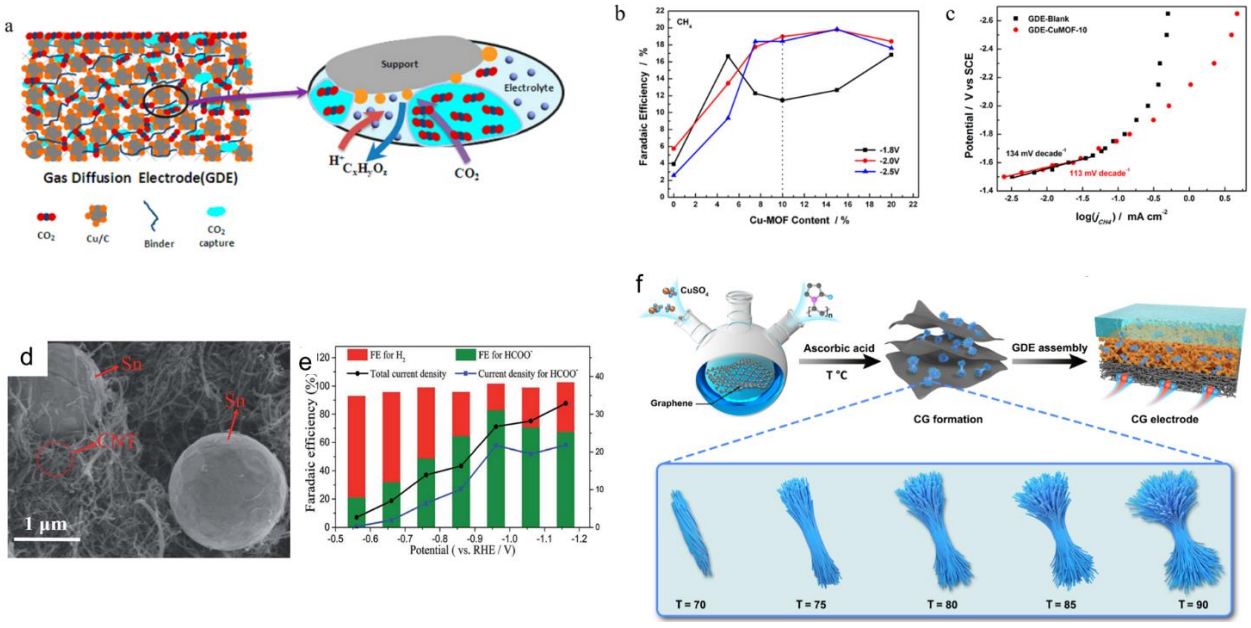


**Figure 11.** (a) Structural schematic diagram of GDE with $Cu_3(BTC)_2$ (b) Effect of content of Cu-MOF on the faradaic efficiency of $CH_4$ after 15 min electrolysis at constant potentials in $CO_2$ saturated 0.5 M $NaHCO_3$ (c) Tafel plot with linear fit at low current densities for GDE with and without Cu-MOF. Reprinted with permission from [112]. Copyright 2018, American Chemical Society. (d) SEM images of Sn/CNT-Agls, (e) variations of the average current density and faradaic efficiency with the electrolysis potential on the Sn/CNT-Agls/CC electrode.[17] Copyright 2017, Royal Society Chemistry. (f) Scheme of CG electrodes for $eCO_2RR$. i) Modified polyol method for CG synthesis; ii) CG formation on graphene layer; iii) GDE assembly of CG electrode. Enlarged scheme: Morphology of $Cu_2O$ in CG by controlling the reaction temperature from 70 °C to 90 °C, where T (°C) represents the synthesis temperature. [46] Copyright 2022, Elsevier.

3D structure built from 1D and 2D materials embedded with active nanoparticle catalysts is another means of improving the mass transfer of $eCO_2RR$, such as metallic materials, metal nanostructures, and oxide-derived metals (OD-Ms), built into stable and highly porous hierarchical carbon-based 3D structures [114]. Chen et al. [17] developed a 3D structured Sn/CNT-Agls from freeze-drying and calcination for reducing $CO_2$ to formate. The Sn/CNT-Agls exhibited a high specific surface area, superior conductivity, and excellent 3D hierarchical structure (**Fig. 11d**), the resulting catalyst achieved current density of 26.7 mA $cm^{-2}$ with a maximum FE of 82.7% at a moderately applied potential of -0.96 V vs. RHE, as displayed in **Fig. 11e**. Such CNT-Agls play a similar role as GDE but on a microscale, it could alter the $CO_2$ diffusion pathway within the aerogel, keeping reactant retained intimately to active catalyst particles, therefore increase the mass transport.

3D scaffolding structured catalysts: Wang et al. [46] reported a nano-flower shaped $Cu_2O$ on graphene (CG) catalyst which forms a scaffolding catalyst layer assembled on GDE. As shown in **Fig. 11f**, this design significantly enhanced the volume porosity and triple-phase boundary contact area, and the scaffolding structure is believed to enhance the lifetime of the $eCO_2RR$ system due to its enhanced hydrophobicity by increasing the thickness of the catalyst layer. 3D structure also helps in the improvement of the electrode surface, therefore, to reduce the competing water-splitting reaction during $eCO_2RR$. Yue et al. [15] prepared a Cu decorated Sn (Cu/Sn) nanowire 3D catalyst layer structure with a hydrophobic surface by involving trimethoxy (1H, 1H, 2H, 2H-heptadecafluorodecyl) silane (FAS). The hydrophobic electrode achieved a high FE of 94.17% towards HCOOH production at -1.2 V vs. RHE which is over 20% higher than the ordinary electrode, the synthesized electrode achieved an excellent activity for $CO_2$ conversion even at high overpotential ($FE_{HCOOH}$-86.39%, $j_{HCOOH}$-23.95 mA $cm^{-2}$, at -1.4 V vs. RHE), which far exceeded other most of Sn materials.

### *3.2.2 Strategies to Improve $eCO_2RR$ Performance*

**Particle size influence** – An advantageous approach to rise active sites for $eCO_2RR$ and avoid mass transfer limit issues is to employ smaller-size catalysts, for example, atoms on the corners, along the edges and in the crystal planes on the surface of nanoparticles in electrocatalyst nanoparticles have more coordination numbers and chemical interaction energy than their bulk electrocatalysts. Size-dependent $eCO_2RR$ investigations indicated that undercoordinated corner sites produce $H_2$, and edge sites reduce $CO_2$ [115]. Nanomaterials with smaller sizes expose a higher proportion of edge and corner sites, which might bind adsorbates stronger than terrace sites [116]. Such adsorption could facilitate the improvement of FE and alter the rate determining step of $eCO_2RR$. Consequently, it is in principle possible to tune $eCO_2RR$'s performance by adjusting the size of electrocatalysts and pore size, which can be achieved from the multi-processing preparation. Sun et al. [117] explored monodispersed Au nanoparticles with different sizes (4, 6, 8, 10 nm) toward $eCO_2RR$, as shown in **Fig. 12a**. They found that among NPs with four different particle sizes, the 8 nm Au NPs show the maximum FE (up to 90% at -0.67 V vs. RHE, **Fig. 12b**). The smaller Au NPs produced higher overall mass activity, and a maximum CO partial mass activity of 14 A $g^{-1}_{catalyst}$ is observed for 4 nm Au NPs at -0.9 V vs. RHE in 0.5 M $CO_2$-saturated $KHCO_3$ (Fig. 14c), however, smaller Au NPs produce more $H_2$. DFT investigations imply that more edge sites (active for CO production) than corner sites (active

for the competitive HER) on the Au NP surface promote the stabilization of the reduction intermediates, such as COOH*, and the conversion of CO (**Fig. 12d-e**).

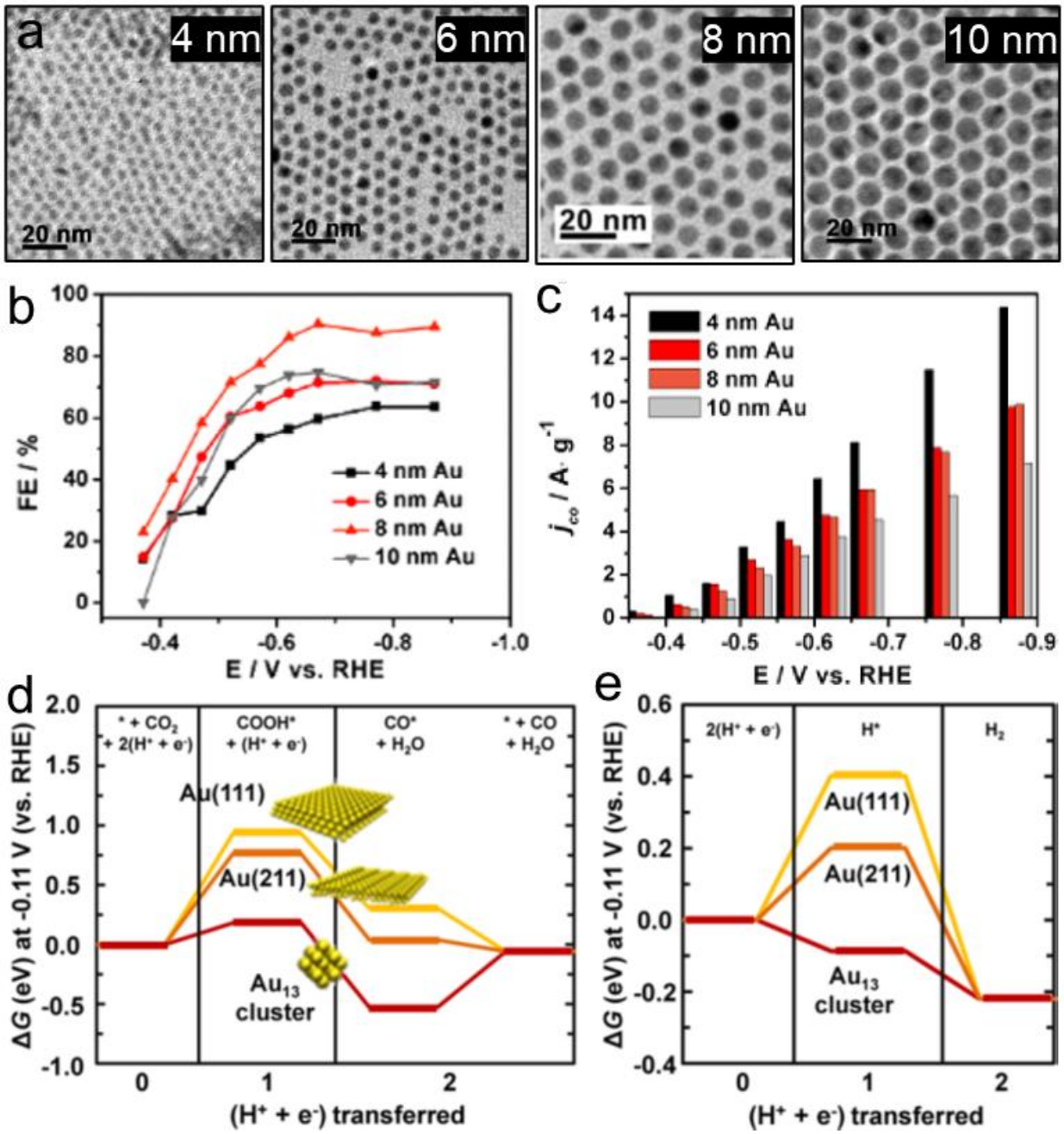


**Figure 12.** (a) TEM images of different Au NPs, (b) Potential-dependent FEs of the C-Au on electrocatalytic reduction of $CO_2$ to CO, (c) Current densities for CO formation (mass activities) on the C-Au at various potentials. Free energy diagrams for electrochemical reduction of (d) $CO_2$ to CO and (e) protons to hydrogen on Au (111) (yellow symbols), Au (211) (orange symbols), or a 13-atom Au cluster (red symbols) at −0.11 V. Reprinted with permission from [117]. Copyright 2013, American Chemical Society.

**Pore structures** – Porous materials play an important role in the diffusion of $CO_2$ in aqueous solutions due to their special porous structure [118]. The pore size, pore-volume, and interconnected structure, composed of the

combination of different pore distributions (including macropores, mesopores, and micropores), affects the adsorption and diffusion dynamics of $CO_2$ deeply [119]. Several carbon-based catalysts could present a number of active sites for $CO_2$ adsorption owing to the increased pore amounts and decrease in pore size. For example, Jiang et al. [120] reported that the Ni-N-doped porous interconnected carbon (NiNPIC) was rapidly synthesized by an ultrasonic-assisted method for e$CO_2$RR. The high surface area, as well as interconnected porous structures of the catalysts, provide highly accessible Ni-N sites and convenient channels for mass diffusion, which gives rise to better mass transfer, lower interface resistance and high electrolyte/gases transport in the e$CO_2$RR [120].

**Grain boundary** – Metastable grain boundaries (GBs) can act as active e$CO_2$RR sites and have motivated the search for porous structures for better control of mass transfer and reaction routes [91]. As previously demonstrated, Li et al. [91] reported the performance of e$CO_2$RR can be improved by increasing the density of grain boundaries, wire-in-tube (WIT) $SnO_2$ with higher surface area and larger portion of GBs than commercial NP $SnO_2$ is prepared using electrospinning and calcination, which provided the special atomic structure and favourable electron transport of GBs to stabilize the active surfaces of the electrocatalysts, as shown in **Fig. 9g**. Lou et al. [121] synthesized sub-2 nm $SnO_2$ quantum wires (QWs) composed of individual QDs and various GBs on the surface and examined for e$CO_2$RR toward HCOOH conversion. The ultrathin $SnO_2$ QWs with exposed GBs show enhanced current density, improved FE of over 80 % for HCOOH and ca. 90 % for $C_1$ products in a wide potential window than $SnO_2$ NPs. Kumar et al. [118] also reported that the $SnO_2$ porous nanowires with a high density of GBs can improve $CO_2$ reduction performance toward HCOOH. This improvement in $FE_{HCOOH}$ (≈80%) is ascribed to the broken local spatial symmetry near the GBs that regulated the binding energy of the reaction intermediate. Nevertheless, it remains very challenging to explicitly clarify the correlation between GBs and the enhanced reactivity in nanomaterials with low dimensions. Structural defects such as GBs can further create more active sites for electrochemical reactions. Besides, theoretical calculations demonstrated that the broken local spatial symmetry adjacent to the GB can adjust the binding energies of several intermediates, and consequently accelerate $CO_2$ toward value-added chemicals conversion.

**Heteroatom doping** – Heteroatoms incorporation into electrocatalysts, which is also referred to as doping (e.g. B, N, and S), is an approach to alter the electronic structure to achieve enhanced electrochemical activity of pristine carbon [21, 89, 92, 95, 96, 98, 102, 105, 122]. Because the heteroatom incorporation (including heteroatom single-, co-, and multiple-doping) effectively regulates the electronic structure of the carbon. The change of electronic structure is advantageous to endow carbon with an optimized charge-carrier concentration and provide abundant catalytic active sites, therefore, increasing the mass transport of e$CO_2$RR. More recently, N-doped graphene has also been demonstrated as an efficient catalyst for the electrochemical reduction of $CO_2$ to $C_1$ products in aqueous electrolytes, as depicted in **Table 3**. For example, just as the fore-mentioned example [102], the authors prepared nitrogen-doped Fe-Graphene for e$CO_2$RR by employing graphene oxide, $FeCl_3$ and $Ar/NH_3$ atmosphere under high temperature. Fe-$N_4$ structure (M-$N_4$, M refers to metal) and N-doping were considered efficient strategies in the enhancement of $CO_2$ conversion from previous investigations [123, 124]. The introduction of trace Fe atoms in N-doped graphene can generate Fe-$N_4$ moieties, promoting the adsorption of intermediate $COOH^*$ and accelerating the

formation of CO (**Fig. 10g**) [102]. Apparently, heteroatom doping can be a powerful approach to adjusting the structural, electrical, and physicochemical properties of 2D graphene and other similar structures, thereby fully developing its potential for $eCO_2RR$.

**Table 3** $eCO_2RR$ performance of N-doped electrocatalysts.

| Electrocatalysts | FE/% | Reduction product | Ref. |
|---|---|---|---|
| Carbon nanotube arrays | 80 | CO | [95] |
| Fe-graphene | 80 | CO | [102] |
| Sn-carbon nanofibers | 91 | CO | [125] |
| PC61BM[a] | 91.2 | $HCOO^-$ | [16] |
| Pt-GO[b] | 41 | $CH_3OH$ | [126] |

a: (6,6)-phenyl-C61-butyric acid methyl ester

b: graphene oxide

**Anion vacancies** – investigations on introducing anion vacancies in catalysts to improve $eCO_2RR$ performance has been developed. As shown in **Table 4**. Zeng et al. [127] prepared ZnO catalyst with rich oxygen vacancies, and this electrocatalyst exhibited the electrochemical reduction of $CO_2$ into CO with the FE of 83% at -1.1 V vs. RHE, whereas it is only 44% (FE, measured under the same conditions) for pristine ZnO. Huang et al. [128] reported a class of O-vacancy engineered $InO_x$ nanoribbons (NRs) for high performance of $eCO_2RR$ with different O-vacancy concentrations through controlling calcination conditions. In their study, high O-vacancy concentrations give $InO_x$ NRs with excellent $FE_{HCOOH}$ of over 80% at broad potential values and maximized FE of 91.7% with high current density, the mechanistic study also suggested that the rich O-vacancies improve the activity of H-$InO_x$ NRs due to the enhanced $CO_2$ adsorption and activation which was brought from vacancies. DFT analysis and experimental results have demonstrated that the existence of anion vacancies in catalysts facilitates the $CO_2$ adsorption, furthermore, the metal sites near to anion vacancies are more conducive to efficient activation of $CO_2$ to $^*CO_2^{\bullet-}$. It is also confirmed that the anionic vacancies can alter the electronic structure of the material surface and help to reduce the reaction energy barrier. For example, Peng et al. [129] demonstrated sulfur vacancies (S-vacancies) are in-situ produced on the catalyst (CdS-CNTs) surface with a high FE of 95% in the electrochemical reduction of $CO_2$ to CO. A possible reaction mechanism of $eCO_2RR$ on CdS-CNTs was proposed that the $CO_2$ molecule firstly adsorbs on CdS-CNTs at the starting of $eCO_2RR$. Then, the $CO_2$ is reduced to CO by the following three steps: (1) $CO_2$ is reduced to $COOH^*$ by one proton and one electron; (2) The $COOH^*$ is converted into $CO^*$ and $H_2O$ by one proton and one electron; (3) Finally, the $CO^*$ desorbs from CdS-CNTs and converts into CO. The catalytic activity of $eCO_2RR$ to CO improves significantly and the charge-transfer resistance decreases as the increase of S-vacancies due to the formation of S-vacancies. It tunes the electron density of the catalyst surface, and decreases the energy barriers for the second step, promoting $eCO_2RR$ efficiently. DFT investigations verify that the electrochemical $CO_2RR$ to CO is more thermodynamically feasible with the presence of S-vacancy, keeping consistent with the experimental results of $eCO_2RR$ (**Fig. 13a-b**).

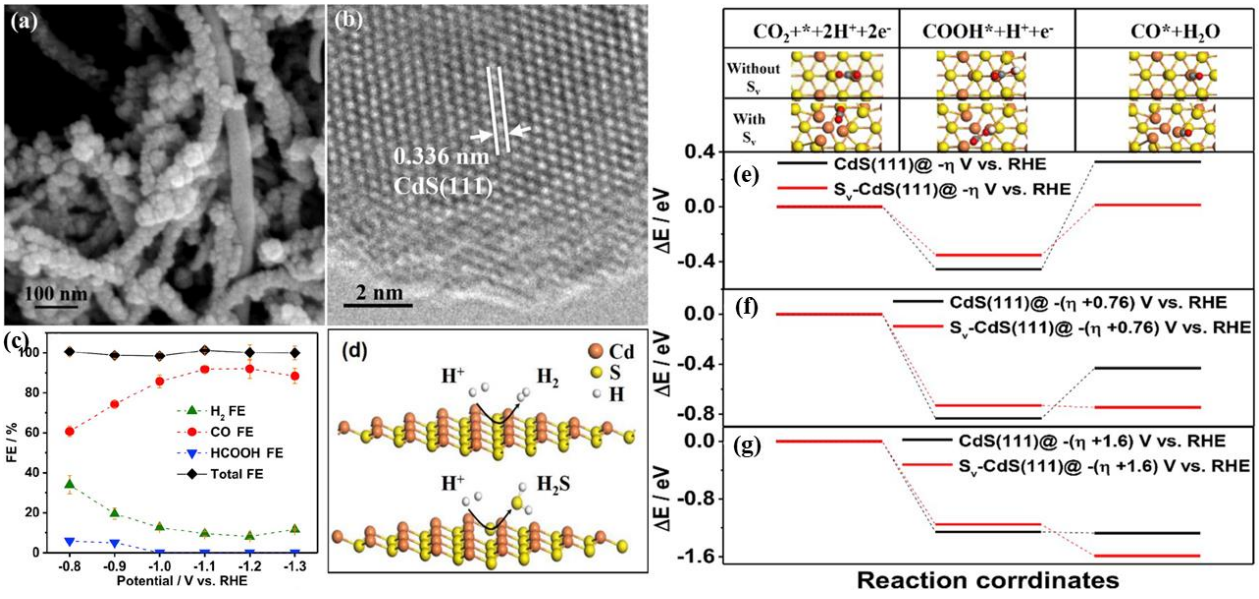


**Figure 13.** (a) SEM image of CdS-CNTs, (b) interplanar lattice fringe spacing in HRTEM images of CdS-CNTs, (c) FEs of $H_2$, CO and HCOOH for $eCO_2RR$ with different potentials on CdS-CNTs, (d) A possible explanation of formation of S-vacancy on the surface of CdS-CNTs during $eCO_2RR$ (e-g) DFT calculation results of relative energy for possible intermediates during $eCO_2RR$ on CdS(111) without S-vacancy and CdS(111) with S vacancy (Sv) at different potentials. [129] Copyright 2019, Elsevier.

**Table 4** $eCO_2RR$ performance of anion vacancies in electrocatalysts.

| Type of anion vacancy | Electrocatalysts | FE/% | Reduction product | Ref. |
|---|---|---|---|---|
| Oxygen | ZnO nanosheets | 83 | CO | [127] |
| Oxygen | $InO_x$ | 91.7 | HCOOH | [128] |
| Oxygen | Cu-$CeO_2$ | 58 | $CH_4$ | [130] |
| Oxygen | $Co_3O_4$ | 85 | HCOOH | [131] |
| Sulfur | CdS-CNTs | 95 | CO | [129] |

**Other strategies** – Many efforts have been developed for improving selectivity, efficiency, and durability for $eCO_2RR$. Not limited to the above strategies, several new approaches are also applied in $eCO_2RR$ $eCO_2RR$application, except the aforementioned heteroatom doping, anion vacancies, etc. The functionalized group introduced on the electrocatalyst also can improve the performance of $eCO_2RR$. For example, Gong et al. [132] demonstrated surface hydroxy (-OH) groups have a great influence on the $Cu_2O$ octahedra electrocatalysts towards $eCO_2RR$ and HER. Theoretically analysis was employed that the charge transfer from hydroxy groups to coordination-unsaturated Cu sites which were assumed as active sites, stabilizing surface-adsorbed COOH*, which is a crucial intermediate in multi-steps of $eCO_2RR$. Furthermore, the performance of $eCO_2RR$ was assessed over $Cu_2O$ octahedral catalysts with {111} facets and different surface coverages of -OH groups. As a result, catalysts with mild coverage of -OH groups can indeed enhance the $eCO_2RR$ and repress HER by combing experimentally

and theoretical investigations. Similarly, Lv et al. [133] proposed a strategy of building fluorosilane-modified $MoS_2$ nanosheets with a hydrophobic surface that exfoliated from bulk $MoS_2$. First, the electron properties of the edge Mo atom can be tuned through the introduced flurosilane group. And then, the hydrophobic surface can suppress HER, whilst generating a great three-phase interface for e$CO_2$RR. The above advantages facilitate the rate-limiting step of CO desorption and enhance e$CO_2$RR process. Another approach to enhance the performance of e$CO_2$RR is through alloying strategy [134, 135], with the background that bulk metals have been investigated widely as e$CO_2$RR electrocatalysts, as shown in **Fig. 4**. This strategy can alter the electronic and chemical properties of metals through the intimate interaction and special structure configuration of metals. Here is a typical example, Cu is one of the most widely studied metals for e$CO_2$RR than other bulk metals because it produces a range distribution of useful chemicals, including CO, formate, ethanol, and even larger $C_3$-$C_4$ chemicals. However, Cu does not produce those chemicals with high selectivity.

### 3.3 Electrolyte

The electrolyte is a necessary component for typical electrochemical e$CO_2$RR, it is to provide a medium to transfer protons. The types and properties of electrolytes could affect the reactivity of e$CO_2$RR. For instance, $H_2O$ is an electrolyte with a high proton concentration; the solubility of $CO_2$ in methanol is 5-fold more than that in water under the same conditions [24]. Ionic liquids (ILs) also can promote the e$CO_2$RR in comparison with conventional aqueous and organic electrolytes due to promoting the adsorption of $CO_2$ on the catalyst surface. In this section, the electrolyte's role and the relationship between the mass transfer of $CO_2$ and electrolyte will be discussed with several examples.

#### *3.3.1 Aqueous Electrolyte*

The most commonly used aqueous electrolytes are $CO_2$-saturated bicarbonate ($NaHCO_3$ or $KHCO_3$, pH = 7.0) with different concentrations, $H_2O$ is often selected as it maintains a high proton concentration. The pH value is controlled for $CO_2$RR, it means that proton concentration can be tuned and used for suppressing the undesired HER. Here, the bicarbonate electrolyte was also selected considering it can act as a buffer to maintain the pH value to some extent. However, the solubility of $CO_2$ in bicarbonate electrolytes is not favourable, this is not good for $CO_2$ transportation in electrolytes and catalysts compared with organic electrolytes. Saveant et al. [136] studied the effect of cations ($Mg^{2+}$, $Li^+$, $Na^+$, etc.) on electrochemical e$CO_2$RR by Fe-based porphyrins. They concluded that the performance of e$CO_2$RR was in the sequence $Mg^{2+}$= $Ca^{2+}$> $Ba^{2+}$> $Li^+$>$Na^+$ due to the introduction of Lewis acid cations provided electrophilic assistance to promote the breaking of one of the C=O bonds of carbon dioxide molecules. However, the selectivity of reduction products is unchanged through the change in the electrolyte, which indicates that the cations did not affect the reaction pathways and negligible impact on the mass transfer of $CO_2$ during e$CO_2$RR [137].

#### *3.3.2 Non-aqueous Electrolyte*

Organic electrolyte has good advantages, such as good solubility of $CO_2$, and less mobility of proton. For example, methanol ($CH_3OH$) is a kind of popular organic electrolyte in e$CO_2$RR, especially, the solubility of $CO_2$ in

$CH_3OH$ is approximately 5-fold higher than that in water under the same conditions [24]. In methanol solution, HER could also be suppressed due to the decreased concentration of $H^+$ ions [138]. As a result, selecting methanol-based electrolytes for $eCO_2RR$ is a beneficial option. Kaneco et al. [138] demonstrated that the FE of hydrocarbons on Cu electrodes could reach more than 80% compared with $eCO_2RR$ in an aqueous solution (30% FE) as methanol was selected as an electrolyte under the same conditions, especially, the introduction of secondary electrolytes could change obviously the mass transport and the selectivity of reduction targets. Before that, Kaneco and co-workers continued to investigate the effect of anionic species on the electrochemical $eCO_2RR$ with Cu electrodes in methanol/aqueous electrolyte, as shown in **Table 5**. And they found the selectivity of ethylene formation over methane increased in the sequence bromide>iodide>chloride>thiocyanate>acetate [139]. However, the selectivity of $eCO_2RR$ is also limited in several organic solvents due to the reason of low proton concentration [140]. A typical example is, the formation of formate that $CO_2$ reacted with protons was severely suppressed in 0.1 M TEAP/$H_2O$ (tetraethylammonium perchlorate, TEAP) [141].

**Table 5** Ratios of typical faradaic efficiency of methane and ethylene in the electrochemical reduction of $CO_2$ at Cu electrode [138].

| Cation of supporting salts | FE/% | | | | | | | |
|---|---|---|---|---|---|---|---|---|
| | Methanol | | | | Water | | | |
| | $CH_4$ | $C_2H_4$ | Total | Ratio | $CH_4$ | $C_2H_4$ | Total | Ratio |
| Li (−503, −100.8) | 63.0 | 14.7 | 77.7 | 4.3 | 26 | 4 | 30 | 6.5 |
| Na (−404, −69) | 63.0 | 17.6 | 80.6 | 3.6 | 19 | 11 | 30 | 1.7 |
| K (−320, −34) | 16.0 | 37.5 | 53.5 | 0.43 | 16 | 14 | 30 | 1.1 |
| Rb (−290, −22) | 4.6 | 31.0 | 35.6 | 0.15 | - | - | - | - |
| Cs (−259, −18) | 4.1 | 32.7 | 36.8 | 0.13 | 15 | 13 | 28 | 1.2 |

### *3.3.3 Ionic Liquid Electrolyte*

Ionic liquids (ILs) and ILs with supporting electrolytes of inorganic salts and organic solvents have been intensively used as liquid electrolytes in $eCO_2RR$ [142]. ILs can definitely facilitate the $eCO_2RR$ compared with typical aqueous (bicarbonate salts) or organic electrolytes (methanol/alcohol, etc.). ILs also can establish a possible complex based on their cations and the intermediates $CO_2^{\cdot-}$ to decrease the reaction energy barrier that $eCO_2RR$ needs, the reaction rate will be enhanced due to the favourable solubility of $CO_2$ in IL solutions. The structure of ILs can coordinate with $CO_2$ molecules, further enhancing the adsorption of $CO_2$ on the catalyst surface and then promoting the mass transfer of $CO_2$ on the two phases or three phases interface. [10] Therefore, the $CO_2$ conversion efficiency and the selectivity of the reduction product could be improved during the reaction pathways. However, highly porous electrode materials or layered materials with a small interlayer distance were limited and suitable for $eCO_2RR$ due to the low ion mobility and high viscosity of ILs [143, 144]. The anions or cations will also affect the electrochemical activity of $CO_2RR$.

## 4. Summary and Outlook

Electrochemical reduction of $CO_2$ ($eCO_2RR$) into value-added carbon-containing products via green energy (solar, wind and hydrogen, etc.), plays an important role in improving environmental issues and optimizing sustainable energy structure in the future. The mass transfer of $CO_2$ is a non-negligible issue in the $eCO_2RR$ application. In this article, we provide a systematic and comprehensive review of the mass transfer of $CO_2$ and discuss the effect of all components' (system design, electrode, electrocatalyst, and electrolyte) effect on the mass transfer of reduction reaction of $CO_2$. In the end, the following strategies may provide new possibilities for the improvement of $eCO_2RR$.

i) Alternative $eCO_2RR$ reactor structure. Gaseous $CO_2$ is pumped into the cathode side and then diffused to the catalyst layer where $CO_2$ will convert into carbon-based products. A specifically designed reactor can facilitate $CO_2$ diffusion and retain the maximum amount intimately adjacent to the active catalyst sites. The consequence is the increase in $eCO_2RR$ mass transfer, resulting in an improved efficiency/reaction rate of $eCO_2RR$. In addition, tuning the pump circular pace, gas pressure of $CO_2$, and pH value of the electrolyte can also improve the $CO_2$ solubility issue to improve the mass transfer of $eCO_2RR$. mass transfer.

ii) New $eCO_2RR$ electrocatalyst. The key reaction of $eCO_2RR$ is that $CO_2$ reacts with electrocatalyst to form the intermediate product, $CO_2^{\cdot-}$. Experimental and theoretical investigations for catalysts should perform together to get insights on the mechanism of $eCO_2RR$. More active sites on the catalyst can make $eCO_2RR$ more efficient. Strategies on introducing active sites will facilitate the reaction process, such as defects engineering (*e.g.,* grain boundary, heteroatom doping, anion vacancies, etc.), and surface engineering (*e.g.* size effect) on the nanostructured catalysts. Several catalysts can adsorb $CO_2$ on its surface due to molecular interaction, this phenomenon can also improve the mass transfer of $CO_2$, then increase $CO_2$ conversion efficiency. Therefore, developing new catalysts with adsorption capacity is another realm for $eCO_2RR$ research.

iii) Optimized electrode and electrolyte. The choice of electrode and electrolyte can affect the performance of $eCO_2RR$. Because the formation of adsorbed intermediates and rate-determining steps are influenced by various type of electrolytes. Different electrodes (foil, mesh and GDE) also alter the activity and stability of the catalyst. For more efficient $CO_2$ conversion, the electrode and electrolyte should be further addressed.

iv) In-depth understanding of the $eCO_2RR$ mechanism. In $eCO_2RR$, how $CO_2$ is reduced on the surface of the catalyst is still under discovery. A comprehensive understanding of the reaction mechanism of $eCO_2RR$ may provide answers to these critical questions and allow the rational design of the next generation of $eCO_2RR$ reactor and catalyst. Oppositely, studies on HER are regarded as providing a reverse insight to understand $eCO_2RR$. To further demonstrate the possible reaction mechanism and intermediates of catalysts for $eCO_2RR$, experimental and theoretical investigations should also be made. Coupling with the common characterization techniques (e.g., in situ XPS or operando characterization), is highly recommended as they enable us to probe catalytical reaction occurring at the two phases or three phases interface.

**Acknowledgement**

This work was supported by the UK Engineering Physics and Science Research Council (Grant No. EP/S032886/1) and the Royal Society International Exchanges Award (Grant No. IEC/NSFC/201008) for research support.

**References**

[1] O. Hoegh-Guldberg, D. Jacob, M. Taylor, T.G. Bolanos, M. Bindi, S. Brown, I.A. Camilloni, A. Diedhiou, R. Djalante, K. Ebi, F. Engelbrecht, J. Guiot, Y. Hijioka, S. Mehrotra, C.W. Hope, A.J. Payne, H.O. Portner, S.I. Seneviratne, A. Thomas, R. Warren, G. Zhou, The human imperative of stabilizing global climate change at 1.5 degrees C, Science, 365 (2019) eaaw6974.
[2] T. Wilberforce, A.G. Olabi, E.T. Sayed, K. Elsaid, M.A. Abdelkareem, Progress in carbon capture technologies, Science of the Total Environment, 761 (2021) 143203.
[3] A.I. Osman, M. Hefny, M. Abdel Maksoud, A.M. Elgarahy, D.W. Rooney, Recent advances in carbon capture storage and utilisation technologies: a review, Environmental Chemistry Letters, 19 (2021) 797-849.
[4] J.W. Fu, K.X. Jiang, X.Q. Qiu, J.G. Yu, M. Liu, Product selectivity of photocatalytic $CO_2$ reduction reactions, Materials Today, 32 (2020) 222-243.
[5] G. Zhao, X. Huang, X. Wang, X. Wang, Progress in catalyst exploration for heterogeneous $CO_2$ reduction and utilization: a critical review, Journal of Materials Chemistry A, 5 (2017) 21625-21649.
[6] L. Xing, R.C. Darton, A. Yang, Enhanced weathering to capture atmospheric carbon dioxide: Modeling of a trickle‐bed reactor, AIChE Journal, 67 (2021) e17202.
[7] L. Xing, H. Pullin, L. Bullock, P. Renforth, R.C. Darton, A. Yang, Potential of enhanced weathering of calcite in packed bubble columns with seawater for carbon dioxide removal, Chemical Engineering Journal, 431 (2022) 134096.
[8] Z. Yang, D. Li, L. Xing, H. Xiang, J. Xuan, S. Cheng, E.H. Yu, A. Yang, Modeling and upscaling analysis of gas diffusion electrode-based electrochemical carbon dioxide reduction systems, ACS Sustainable Chemistry & Engineering, 9 (2020) 351-361.
[9] J. Wu, S. Ma, J. Sun, J.I. Gold, C. Tiwary, B. Kim, L. Zhu, N. Chopra, I.N. Odeh, R. Vajtai, A.Z. Yu, R. Luo, J. Lou, G. Ding, P.J. Kenis, P.M. Ajayan, A metal-free electrocatalyst for carbon dioxide reduction to multi-carbon hydrocarbons and oxygenates, Nature Communications, 7 (2016) 13869.
[10] Q. Lu, F. Jiao, Electrochemical $CO_2$ reduction: Electrocatalyst, reaction mechanism, and process engineering, Nano Energy, 29 (2016) 439-456.
[11] P. Lobaccaro, M.R. Singh, E.L. Clark, Y. Kwon, A.T. Bell, J.W. Ager, Effects of temperature and gas-liquid mass transfer on the operation of small electrochemical cells for the quantitative evaluation of $CO_2$ reduction electrocatalysts, Physical Chemistry Chemical Physics, 18 (2016) 26777-26785.
[12] J. Qiao, Y. Liu, J. Zhang, Electrochemical reduction of carbon dioxide: fundamentals and technologies, CRC Press2016.
[13] J. Zhang, PEM Fuel Cell Electrocatalysts and Catalyst Layers, Springer Science & Business Media2008.
[14] N. Sonoyama, M. Kirii, T. Sakata, Electrochemical reduction of $CO_2$ at metal-porphyrin supported gas diffusion electrodes under high pressure $CO_2$, Electrochemistry Communications, 1 (1999) 213-216.
[15] P.T. Yue, Q. Fu, J. Li, L. Zhang, L. Xing, Z.Y. Kang, Q. Liao, X. Zhu, Triple-phase electrocatalysis for the enhanced $CO_2$ reduction to HCOOH on a hydrophobic surface, Chemical Engineering Journal, 405 (2021) 126975.
[16] Z.P. Chen, K.W. Mou, S.Y. Yao, L.C. Liu, Highly selective electrochemical reduction of $CO_2$ to formate on metal-free nitrogen-doped PC61BM, Journal of Materials Chemistry A, 6 (2018) 11236-11243.

[17] Z.P. Chen, S.Y. Yao, L.C. Liu, 3D hierarchical porous structured carbon nanotube aerogel-supported Sn spheroidal particles: an efficient and selective catalyst for electrochemical reduction of $CO_2$ to formate, Journal of Materials Chemistry A, 5 (2017) 24651-24656.
[18] H. Zhong, K. Fujii, Y. Nakano, F. Jin, Effect of $CO_2$ Bubbling into Aqueous Solutions Used for Electrochemical Reduction of $CO_2$ for Energy Conversion and Storage, The Journal of Physical Chemistry C, 119 (2014) 55-61.
[19] M. Rahaman, A. Dutta, A. Zanetti, P. Broekmann, Electrochemical Reduction of $CO_2$ into Multicarbon Alcohols on Activated Cu Mesh Catalysts: An Identical Location (IL) Study, ACS Catalysis, 7 (2017) 7946-7956.
[20] D. Higgins, C. Hahn, C. Xiang, T.F. Jaramillo, A.Z. Weber, Gas-diffusion electrodes for carbon dioxide reduction: a new paradigm, ACS Energy Letters, 4 (2018) 317-324.
[21] X. Cui, Z. Pan, L. Zhang, H. Peng, G. Zheng, Selective Etching of Nitrogen-Doped Carbon by Steam for Enhanced Electrochemical $CO_2$ Reduction, Advanced Energy Materials, 7 (2017) 1701456.
[22] B. Endrodi, G. Bencsik, F. Darvas, R. Jones, K. Rajeshwar, C. Janaky, Continuous-flow electroreduction of carbon dioxide, Progress in Energy and Combustion Science, 62 (2017) 133-154.
[23] J.T. Song, H. Song, B. Kim, J. Oh, Towards Higher Rate Electrochemical $CO_2$ Conversion: From Liquid-Phase to Gas-Phase Systems, Catalysts, 9 (2019) 224.
[24] L. Zhang, Z.J. Zhao, J. Gong, Nanostructured Materials for Heterogeneous Electrocatalytic $CO_2$ Reduction and their Related Reaction Mechanisms, Angewandte Chemie International Edition, 56 (2017) 11326-11353.
[25] A.J. Martin, G.O. Larrazabal, J. Perez-Ramirez, Towards sustainable fuels and chemicals through the electrochemical reduction of $CO_2$: lessons from water electrolysis, Green Chemistry, 17 (2015) 5114-5130.
[26] D.D. Zhu, J.L. Liu, S.Z. Qiao, Recent Advances in Inorganic Heterogeneous Electrocatalysts for Reduction of Carbon Dioxide, Advanced Materials, 28 (2016) 3423-3452.
[27] X. Lu, D.Y.C. Leung, H.Z. Wang, J. Xuan, A high performance dual electrolyte microfluidic reactor for the utilization of $CO_2$, Applied Energy, 194 (2017) 549-559.
[28] S.C. Ma, M. Sadakiyo, R. Luo, M. Heima, M. Yamauchi, P.J.A. Kenis, One-step electrosynthesis of ethylene and ethanol from $CO_2$ in an alkaline electrolyzer, Journal of Power Sources, 301 (2016) 219-228.
[29] H. Xiang, S. Rasul, K. Scott, J. Portoles, P. Cumpson, H.Y. Eileen, Enhanced selectivity of carbonaceous products from electrochemical reduction of $CO_2$ in aqueous media, Journal of $CO_2$ Utilization, 30 (2019) 214-221.
[30] Y. Hori, A. Murata, R. Takahashi, Formation of Hydrocarbons in the Electrochemical Reduction of Carbon-Dioxide at a Copper Electrode in Aqueous-Solution, J Chem Soc Farad T 1, 85 (1989) 2309-2326.
[31] B. Kumar, M. Llorente, J. Froehlich, T. Dang, A. Sathrum, C.P. Kubiak, Photochemical and photoelectrochemical reduction of $CO_2$, Annual Review of Physical Chemistry, 63 (2012) 541-569.
[32] A.A. Peterson, F. Abild-Pedersen, F. Studt, J. Rossmeisl, J.K. Norskov, How copper catalyzes the electroreduction of carbon dioxide into hydrocarbon fuels, Energy & Environmental Science, 3 (2010) 1311-1315.
[33] S. Zarghami, F. Boukadi, Y. Al-Wahaibi, Diffusion of carbon dioxide in formation water as a result of $CO_2$ enhanced oil recovery and $CO_2$ sequestration, Journal of Petroleum Exploration and Production Technology, 7 (2016) 161-168.
[34] J. Resasco, L.D. Chen, E. Clark, C. Tsai, C. Hahn, T.F. Jaramillo, K. Chan, A.T. Bell, Promoter Effects of Alkali Metal Cations on the Electrochemical Reduction of Carbon Dioxide, J Am Chem Soc, 139 (2017) 11277-11287.
[35] S. Park, J.W. Lee, B.N. Popov, A review of gas diffusion layer in PEM fuel cells: Materials and designs, International Journal of Hydrogen Energy, 37 (2012) 5850-5865.

[36] Y. Bultel, P. Ozil, R. Durand, Modelling of mass transfer within the PEM fuel cell active layer: limitations at the particle level, Journal of Applied Electrochemistry, 29 (1999) 1025-1033.
[37] I. Dumitrescu, R.M. Crooks, Effect of mass transfer on the oxygen reduction reaction catalyzed by platinum dendrimer encapsulated nanoparticles, Proceedings of the National Academy of Sciences, 109 (2012) 11493-11497.
[38] W. Lee, Y.E. Kim, M.H. Youn, S.K. Jeong, K.T. Park, Catholyte-Free Electrocatalytic $CO_2$ Reduction to Formate, Angewandte Chemie International Edition, 57 (2018) 6883-6887.
[39] A. Patru, T. Binninger, B. Pribyl, T.J. Schmidt, Design Principles of Bipolar Electrochemical Co-Electrolysis Cells for Efficient Reduction of Carbon Dioxide from Gas Phase at Low Temperature, Journal of the Electrochemical Society, 166 (2019) F34-F43.
[40] C.T. Dinh, T. Burdyny, M.G. Kibria, A. Seifitokaldani, C.M. Gabardo, F.P. Garcia de Arquer, A. Kiani, J.P. Edwards, P. De Luna, O.S. Bushuyev, C. Zou, R. Quintero-Bermudez, Y. Pang, D. Sinton, E.H. Sargent, $CO_2$ electroreduction to ethylene via hydroxide-mediated copper catalysis at an abrupt interface, Science, 360 (2018) 783-787.
[41] C.M. Gabardo, A. Seifitokaldani, J.P. Edwards, C.T. Dinh, T. Burdyny, M.G. Kibria, C.P. O'Brien, E.H. Sargent, D. Sinton, Combined high alkalinity and pressurization enable efficient $CO_2$ electroreduction to CO, Energy & Environmental Science, 11 (2018) 2531-2539.
[42] E.J. Dufek, T.E. Lister, S.G. Stone, M.E. McIlwain, Operation of a Pressurized System for Continuous Reduction of $CO_2$, Journal of the Electrochemical Society, 159 (2012) F514-F517.
[43] E.J. Dufek, T.E. Lister, S.G. Stone, Sampling dynamics for pressurized electrochemical cells, Journal of Applied Electrochemistry, 44 (2014) 849-855.
[44] D. Mignard, R.C. Batik, A.S. Bharadwaj, C.L. Pritchard, M. Ragnoli, F. Cecconi, H. Miller, L.J. Yellowlees, Revisiting strontium-doped lanthanum cuprate perovskite for the electrochemical reduction of $CO_2$, Journal of $CO_2$ Utilization, 5 (2014) 53-59.
[45] G. Wang, J. Pan, S.P. Jiang, H. Yang, Gas phase electrochemical conversion of humidified $CO_2$ to CO and $H_2$ on proton-exchange and alkaline anion-exchange membrane fuel cell reactors, Journal of $CO_2$ Utilization, 23 (2018) 152-158.
[46] Y. Wang, H. Lei, S. Lu, Z. Yang, B.B. Xu, L. Xing, T.X. Liu, $Cu_2O$ Nano-flowers/Graphene Enabled Scaffolding Structure Catalyst Layer for Enhanced $CO_2$ Electrochemical Reduction, Applied Catalysis B: Environmental, (2021) 121022.
[47] A. Del Castillo, M. Alvarez-Guerra, J. Solla-Gullón, A. Sáez, V. Montiel, A. Irabien, Sn nanoparticles on gas diffusion electrodes: Synthesis, characterization and use for continuous $CO_2$ electroreduction to formate, Journal of $CO_2$ Utilization, 18 (2017) 222-228.
[48] R.B. Kutz, Q. Chen, H. Yang, S.D. Sajjad, Z. Liu, I.R. Masel, Sustainion Imidazolium‐Functionalized Polymers for Carbon Dioxide Electrolysis, Energy Technology, 5 (2017) 929-936.
[49] Y. Wang, H. Lei, H. Xiang, Y. Fu, C. Xu, Y. Jiang, B.B. Xu, E.H. Yu, C. Gao, T.X. Liu, Porous Bilayer Electrode‐Guided Gas Diffusion for Enhanced $CO_2$ Electrochemical Reduction, Advanced Energy and Sustainability Research, 2 (2021) 2100083.
[50] H.P. Yang, Q. Lin, H.W. Zhang, Y. Wu, L.D. Fan, X.Y. Chai, Q.L. Zhang, J.H. Liu, C.X. He, Selective electrochemical reduction of $CO_2$ by a binder-free platinum/nitrogen-doped carbon nanofiber/copper foil catalyst with remarkable efficiency and reusability, Electrochemistry Communications, 93 (2018) 138-142.
[51] W. Ju, F. Jiang, H. Ma, Z. Pan, Y.B. Zhao, F. Pagani, D. Rentsch, J. Wang, C. Battaglia, Electrocatalytic Reduction of Gaseous $CO_2$ to CO on Sn/Cu‐Nanofiber‐Based Gas Diffusion Electrodes, Advanced Energy Materials, 9 (2019) 1901514.
[52] M.J.E. B. J. Seddon, A. Firth, A. E. Owen and H. H. J. Girault Thin Film Electrode: A New Method for The Fabrication of Submicrometer Band Electrodes, Electrochimica Acta, 36 763-771.

[53] M. Le, M. Ren, Z. Zhang, P.T. Sprunger, R.L. Kurtz, J.C. Flake, Electrochemical reduction of $CO_2$ to $CH_3OH$ at copper oxide surfaces, Journal of the Electrochemical Society, 158 (2011) E45-E49.
[54] K.B. Oldham, C.G. Zoski, Chapter 2 Mass Transport to Electrodes, Electrode Kinetics: Principles and Methodology1986, pp. 79-143.
[55] M.L. Perry, J. Newman, E.J. Cairns, Mass transport in gas-diffusion electrodes: A diagnostic tool for fuel-cell cathodes, Journal of the Electrochemical Society, 145 (1998) 5-15.
[56] T. Burdyny, W.A. Smith, $CO_2$ reduction on gas-diffusion electrodes and why catalytic performance must be assessed at commercially-relevant conditions, Energy & Environmental Science, 12 (2019) 1442-1453.
[57] D.M. Weekes, D.A. Salvatore, A. Reyes, A. Huang, C.P. Berlinguette, Electrolytic $CO_2$ reduction in a flow cell, Accounts of Chemical Research, 51 (2018) 910-918.
[58] A. Bandi, Electrochemical reduction of carbon dioxide on conductive metallic oxides, Journal of the Electrochemical Society, 137 (1990) 2157-2160.
[59] C.W. Li, M.W. Kanan, $CO_2$ Reduction at Low Overpotential on Cu Electrodes Resulting from the Reduction of Thick $Cu_2O$ Films, J Am Chem Soc, 134 (2012) 7231-7234.
[60] Y. Chen, M.W. Kanan, Tin oxide dependence of the $CO_2$ reduction efficiency on tin electrodes and enhanced activity for tin/tin oxide thin-film catalysts, J Am Chem Soc, 134 (2012) 1986-1989.
[61] J. Wu, F.G. Risalvato, F.-S. Ke, P.J. Pellechia, X.-D. Zhou, Electrochemical Reduction of Carbon Dioxide I. Effects of the Electrolyte on the Selectivity and Activity with Sn Electrode, Journal of The Electrochemical Society, 159 (2012) F353-F359.
[62] J. Kim, D. Summers, K. Frese Jr, Reduction of $CO_2$ and CO to methane on Cu foil electrodes, Journal of Electroanalytical Chemistry and Interfacial Electrochemistry, 245 (1988) 223-244.
[63] D.W. Dewulf, T. Jin, A.J. Bard, Electrochemical and Surface Studies of Carbon-Dioxide Reduction to Methane and Ethylene at Copper Electrodes in Aqueous-Solutions, Journal of the Electrochemical Society, 136 (1989) 1686-1691.
[64] W.X. Lv, J. Zhou, J.J. Bei, R. Zhang, L. Wang, Q. Xu, W. Wang, Electrodeposition of nano-sized bismuth on copper foil as electrocatalyst for reduction of $CO_2$ to formate, Applied Surface Science, 393 (2017) 191-196.
[65] Y. Hori, K. Kikuchi, A. Murata, S. Suzuki, Production of Methane and Ethylene in Electrochemical Reduction of Carbon Dioxide at Copper Electrode in Aqueous Hydrogencarbonate Solution, Chemistry Letters, 15 (1986) 897-898.
[66] K.K. Yoshio HORI, and Shin SUZUKI, Production of CO and $CH_4$ in electrochemical reduction of $CO_2$ at metal electrodes in aqueous hydrogencarbonate solution, Chemistry Letters, (1985) 1695-1698.
[67] D. Rochefort, P. Dabo, D. Guay, P.M.A. Sherwood, XPS investigations of thermally prepared $RuO_2$ electrodes in reductive conditions, Electrochimica Acta, 48 (2003) 4245-4252.
[68] C.Y. Falong Jia, Kejian Deng, and Lizhi Zhang, Nanoporous Metal (Cu, Ag, Au) Films with High Surface Area: General Fabrication and Preliminary Electrochemical Performance, The Journal of Physical Chemistry, 111 (2007) 8424-8431.
[69] C. Chen, B. Zhang, J. Zhong, Z. Cheng, Selective electrochemical $CO_2$ reduction over highly porous gold films, Journal of Materials Chemistry A, 5 (2017) 21955-21964.
[70] Y. Peng, T. Wu, L. Sun, J.M.V. Nsanzimana, A.C. Fisher, X. Wang, Selective Electrochemical Reduction of $CO_2$ to Ethylene on Nanopores-Modified Copper Electrodes in Aqueous Solution, ACS Applied Materials & Interfaces, 9 (2017) 32782-32789.
[71] G.B. Stevens, T. Reda, B. Raguse, Energy storage by the electrochemical reduction of $CO_2$ to CO at a porous Au film, Journal of Electroanalytical Chemistry, 526 (2002) 125-133.
[72] K. Ogura, H. Yano, T. Tanaka, Selective formation of ethylene from $CO_2$ by catalytic electrolysis at a three-phase interface, Catalysis Today, 98 (2004) 515-521.

[73] S.R. Narayanan, B. Haines, J. Soler, T.I. Valdez, Electrochemical Conversion of Carbon Dioxide to Formate in Alkaline Polymer Electrolyte Membrane Cells, Journal of the Electrochemical Society, 158 (2011) A167-A173.
[74] H. Li, C. Oloman, The electro-reduction of carbon dioxide in a continuous reactor, Journal of Applied Electrochemistry, 35 (2005) 955-965.
[75] H. Yano, F. Shirai, M. Nakayama, K. Ogura, Efficient electrochemical conversion of $CO_2$ to CO, $C_2H_4$ and $CH_4$ at a three-phase interface on a Cu net electrode in acidic solution, Journal of Electroanalytical Chemistry, 519 (2002) 93-100.
[76] H. Li, C. Oloman, Development of a continuous reactor for the electro-reduction of carbon dioxide to formate – Part 1: Process variables, Journal of Applied Electrochemistry, 36 (2006) 1105-1115.
[77] Y. Hirata, K. Suga, M. Fujihira, In situ Analysis of Products in Electrocatalytic Reduction of $CO_2$ with Ni-cyclam by Differential Electrochemical Mass Spectroscopy during Cyclic Voltammetry on an Amalgamated-Gold Mesh Electrode, Chemistry Letters, 19 (1990) 1155-1158.
[78] H. Yano, T. Tanaka, M. Nakayama, K. Ogura, Selective electrochemical reduction of $CO_2$ to ethylene at a three-phase interface on copper(I) halide-confined Cu-mesh electrodes in acidic solutions of potassium halides, Journal of Electroanalytical Chemistry, 565 (2004) 287-293.
[79] A.W. Kahsay, K.B. Ibrahim, M.-C. Tsai, M.K. Birhanu, S.A. Chala, W.-N. Su, B.-J. Hwang, Selective and Low Overpotential Electrochemical $CO_2$ Reduction to Formate on CuS Decorated CuO Heterostructure, Catalysis Letters, 149 (2019) 860-869.
[80] S. Srinivasan, H.D. Hurwitz, J.O.M. Bockris, Fundamental Equations of Electrochemical Kinetics at Porous Gas‐Diffusion Electrodes, The Journal of Chemical Physics, 46 (1967) 3108-3122.
[81] Y. Wang, K.S. Chen, Effect of Spatially-Varying GDL Properties and Land Compression on Water Distribution in PEM Fuel Cells, Journal of the Electrochemical Society, 158 (2011) B1292-B1299.
[82] A. Li, H. Wang, J. Han, L. Liu, Preparation of a Pb loaded gas diffusion electrode and its application to $CO_2$ electroreduction, Frontiers of Chemical Science and Engineering, 6 (2012) 381-388.
[83] F. Bidault, D.J.L. Brett, P.H. Middleton, N.P. Brandon, Review of gas diffusion cathodes for alkaline fuel cells, Journal of Power Sources, 187 (2009) 39-48.
[84] L.C. Weng, A.T. Bell, A.Z. Weber, Towards membrane-electrode assembly systems for $CO_2$ reduction: a modeling study, Energy & Environmental Science, 12 (2019) 1950-1968.
[85] X. Kang, Q. Zhu, X. Sun, J. Hu, J. Zhang, Z. Liu, B. Han, Highly efficient electrochemical reduction of $CO_2$ to $CH_4$ in an ionic liquid using a metal–organic framework cathode, Chemical Science, 7 (2016) 266-273.
[86] Y. Zhu, S. Lu, A.G. Manohari, X.X. Dong, F. Chen, W. Xu, Z.L. Shi, C.X. Xu, Polydopamine interconnected graphene quantum dots and gold nanoparticles for enzymeless $H_2O_2$ detection, Journal of Electroanalytical Chemistry, 796 (2017) 75-81.
[87] X. Cao, C. Shao, C. Zhang, M. Liang, Y. Wang, J. Cheng, S. Lu, Yeast powder derived carbon quantum dots for dopamine detection and living cell imaging, Analytical Methods, 14 (2022) 1342-1350.
[88] Z.P. Zeng, S.F. Chen, T.T.Y. Tan, F.X. Xiao, Graphene quantum dots (GQDs) and its derivatives for multifarious photocatalysis and photoelectrocatalysis, Catalysis Today, 315 (2018) 171-183.
[89] X.L. Zou, M.J. Liu, J.J. Wu, P.M. Ajayan, J. Li, B.L. Liu, B.I. Yakobson, How Nitrogen-Doped Graphene Quantum Dots Catalyze Electroreduction of $CO_2$ to Hydrocarbons and Oxygenates, ACS Catalysis, 7 (2017) 6245-6250.
[90] R. Cheng, Y. Xiang, R. Guo, L. Li, G. Zou, C. Fu, H. Hou, X. Ji, Structure and Interface Modification of Carbon Dots for Electrochemical Energy Application, Small, 17 (2021) e2102091.
[91] L. Fan, Z. Xia, M. Xu, Y. Lu, Z. Li, 1D $SnO_2$ with Wire-in-Tube Architectures for Highly Selective Electrochemical Reduction of $CO_2$ to C1 Products, Advanced Functional Materials, 28 (2018) 1706289.

[92] S. Zhang, P. Kang, S. Ubnoske, M.K. Brennaman, N. Song, R.L. House, J.T. Glass, T.J. Meyer, Polyethylenimine-enhanced electrocatalytic reduction of $CO_2$ to formate at nitrogen-doped carbon nanomaterials, J Am Chem Soc, 136 (2014) 7845-7848.
[93] Q. Wei, F. Xiong, S. Tan, L. Huang, E.H. Lan, B. Dunn, L. Mai, Porous One-Dimensional Nanomaterials: Design, Fabrication and Applications in Electrochemical Energy Storage, Advanced Materials, 29 (2017) 1602300.
[94] B. Kumar, M. Asadi, D. Pisasale, S. Sinha-Ray, B.A. Rosen, R. Haasch, J. Abiade, A.L. Yarin, A. Salehi-Khojin, Renewable and metal-free carbon nanofibre catalysts for carbon dioxide reduction, Nature Communications, 4 (2013) 2819.
[95] P.P. Sharma, J. Wu, R.M. Yadav, M. Liu, C.J. Wright, C.S. Tiwary, B.I. Yakobson, J. Lou, P.M. Ajayan, X.D. Zhou, Nitrogen-Doped Carbon Nanotube Arrays for High-Efficiency Electrochemical Reduction of $CO_2$: On the Understanding of Defects, Defect Density, and Selectivity, Angewandte Chemie International Edition, 54 (2015) 13701-13705.
[96] D.S. Geng, Y. Chen, Y.G. Chen, Y.L. Li, R.Y. Li, X.L. Sun, S.Y. Ye, S. Knights, High oxygen-reduction activity and durability of nitrogen-doped graphene, Energy & Environmental Science, 4 (2011) 760-764.
[97] Q. Li, W.L. Zhu, J.J. Fu, H.Y. Zhang, G. Wu, S.H. Sun, Controlled assembly of Cu nanoparticles on pyridinic-N rich graphene for electrochemical reduction of $CO_2$ to ethylene, Nano Energy, 24 (2016) 1-9.
[98] X. Hong, K.R. Chan, C. Tsai, J.K. Norskov, How Doped $MoS_2$ Breaks Transition-Metal Scaling Relations for $CO_2$ Electrochemical Reduction, ACS Catalysis, 6 (2016) 4428-4437.
[99] Y.F. Zhao, X.D. Jia, G.I.N. Waterhouse, L.Z. Wu, C.H. Tung, D. O'Hare, T.R. Zhang, Layered Double Hydroxide Nanostructured Photocatalysts for Renewable Energy Production, Advanced Energy Materials, 6 (2016) 1501974.
[100] H. Shin, Y. Ha, H. Kim, 2D Covalent Metals: A New Materials Domain of Electrochemical $CO_2$ Conversion with Broken Scaling Relationship, The Journal of Physical Chemistry Letters, 7 (2016) 4124-4129.
[101] H.K. Lim, H. Shin, W.A. Goddard, 3rd, Y.J. Hwang, B.K. Min, H. Kim, Embedding covalency into metal catalysts for efficient electrochemical conversion of $CO_2$, J Am Chem Soc, 136 (2014) 11355-11361.
[102] C. Zhang, S. Yang, J. Wu, M. Liu, S. Yazdi, M. Ren, J. Sha, J. Zhong, K. Nie, A.S. Jalilov, Z. Li, H. Li, B.I. Yakobson, Q. Wu, E. Ringe, H. Xu, P.M. Ajayan, J.M. Tour, Electrochemical $CO_2$ Reduction with Atomic Iron‐Dispersed on Nitrogen‐Doped Graphene, Advanced Energy Materials, 8 (2018) 1703487.
[103] X. Lu, T.H. Tan, Y.H. Ng, R. Amal, Highly Selective and Stable Reduction of $CO_2$ to CO by a Graphitic Carbon Nitride/Carbon Nanotube Composite Electrocatalyst, Chemistry–A European Journal, 22 (2016) 11991-11996.
[104] G. Kresse, J. Furthmuller, Efficient iterative schemes for ab initio total-energy calculations using a plane-wave basis set, Physical Review B, 54 (1996) 11169-11186.
[105] X. Zhi, Y. Jiao, Y. Zheng, S.Z. Qiao, Impact of Interfacial Electron Transfer on Electrochemical $CO_2$ Reduction on Graphitic Carbon Nitride/Doped Graphene, Small, 15 (2019) e1804224.
[106] S. Lu, H. Jia, M. Hummel, Y. Wu, K. Wang, X. Qi, Z. Gu, Two-dimensional conductive phthalocyanine-based metal–organic frameworks for electrochemical nitrite sensing, RSC Advances, 11 (2021) 4472-4477.
[107] N. Kornienko, Y. Zhao, C.S. Kley, C. Zhu, D. Kim, S. Lin, C.J. Chang, O.M. Yaghi, P. Yang, Metal-organic frameworks for electrocatalytic reduction of carbon dioxide, J Am Chem Soc, 137 (2015) 14129-14135.
[108] H. Jia, S. Lu, S.H.R. Shin, M.L. Sushko, X. Tao, M. Hummel, P.K. Thallapally, J. Liu, Z. Gu, In situ anodic electrodeposition of two-dimensional conductive metal-organic framework@nickel foam for high-performance flexible supercapacitor, Journal of Power Sources, 526 (2022) 231163.

[109] S. Lu, M. Hummel, K. Chen, Y. Zhou, S. Kang, Z.R. Gu, Synthesis of Au@ZIF-8 nanocomposites for enhanced electrochemical detection of dopamine, Electrochemistry Communications, 114 (2020) 106715.
[110] H.Y. Liu, J. Chu, Z.L. Yin, X. Cai, L. Zhuang, H.X. Deng, Covalent Organic Frameworks Linked by Amine Bonding for Concerted Electrochemical Reduction of $CO_2$, Chem, 4 (2018) 1696-1709.
[111] D. Britt, D. Tranchemontagne, O.M. Yaghi, Metal-organic frameworks with high capacity and selectivity for harmful gases, Proceedings of the National Academy of Sciences, 105 (2008) 11623-11627.
[112] Y.L. Qiu, H.X. Zhong, T.T. Zhang, W.B. Xu, P.P. Su, X.F. Li, H.M. Zhang, Selective Electrochemical Reduction of Carbon Dioxide Using Cu Based Metal Organic Framework for $CO_2$ Capture, ACS Applied Materials & Interfaces, 10 (2018) 2480-2489.
[113] B.X. Dong, S.L. Qian, F.Y. Bu, Y.C. Wu, L.G. Feng, Y.L. Teng, W.L. Liu, Z.W. Li, Electrochemical Reduction of $CO_2$ to CO by a Heterogeneous Catalyst of Fe-Porphyrin-Based Metal-Organic Framework, ACS Applied Energy Materials, 1 (2018) 4662-4669.
[114] F. Li, L. Chen, G.P. Knowles, D.R. MacFarlane, J. Zhang, Hierarchical Mesoporous $SnO_2$ Nanosheets on Carbon Cloth: A Robust and Flexible Electrocatalyst for $CO_2$ Reduction with High Efficiency and Selectivity, Angewandte Chemie International Edition, 56 (2017) 505-509.
[115] H. Mistry, R. Reske, Z. Zeng, Z.J. Zhao, J. Greeley, P. Strasser, B.R. Cuenya, Exceptional size-dependent activity enhancement in the electroreduction of $CO_2$ over Au nanoparticles, J Am Chem Soc, 136 (2014) 16473-16476.
[116] S. Lu, M. Hummel, Z.R. Gu, Y.C. Wang, K.L. Wang, R. Pathak, Y. Zhou, H.X. Jia, X.Q. Qi, X.H. Zhao, B.B. Xu, X.T. Liu, Highly Efficient Urea Oxidation via Nesting Nano-Nickel Oxide in Eggshell Membrane-Derived Carbon, ACS Sustainable Chemistry & Engineering, 9 (2021) 1703-1713.
[117] W. Zhu, R. Michalsky, O. Metin, H. Lv, S. Guo, C.J. Wright, X. Sun, A.A. Peterson, S. Sun, Monodisperse Au nanoparticles for selective electrocatalytic reduction of $CO_2$ to CO, J Am Chem Soc, 135 (2013) 16833-16836.
[118] B. Kumar, V. Atla, J.P. Brian, S. Kumari, T.Q. Nguyen, M. Sunkara, J.M. Spurgeon, Reduced $SnO_2$ Porous Nanowires with a High Density of Grain Boundaries as Catalysts for Efficient Electrochemical $CO_2$ -into-HCOOH Conversion, Angewandte Chemie International Edition, 56 (2017) 3645-3649.
[119] P.I. Ravikovitch, A. Vishnyakov, R. Russo, A.V. Neimark, Unified Approach to Pore Size Characterization of Microporous Carbonaceous Materials from $N_2$, Ar, and $CO_2$ Adsorption Isotherms, Langmuir, 16 (2000) 2311-2320.
[120] Z.J. Ma, D.P. Wu, X.Y. Han, H.J. Wang, L.M. Zhang, Z.Y. Gao, F. Xu, K. Jiang, Ultrasonic assisted synthesis of Zn-Ni bi-metal MOFs for interconnected Ni-N-C materials with enhanced electrochemical reduction of $CO_2$, Journal of CO2 Utilization, 32 (2019) 251-258.
[121] S. Liu, J. Xiao, X.F. Lu, J. Wang, X. Wang, X.W.D. Lou, Efficient Electrochemical Reduction of $CO_2$ to HCOOH over Sub-2 nm $SnO_2$ Quantum Wires with Exposed Grain Boundaries, Angewandte Chemie International Edition, 58 (2019) 8499-8503.
[122] N. Sreekanth, M.A. Nazrulla, T.V. Vineesh, K. Sailaja, K.L. Phani, Metal-free boron-doped graphene for selective electroreduction of carbon dioxide to formic acid/formate, Chemical Communications, 51 (2015) 16061-16064.
[123] Y. Hou, Y.-L. Liang, P.-C. Shi, Y.-B. Huang, R. Cao, Atomically dispersed Ni species on N-doped carbon nanotubes for electroreduction of $CO_2$ with nearly 100% CO selectivity, Applied Catalysis B: Environmental, 271 (2020) 118929.
[124] S. Cao, S. Wei, X. Wei, S. Zhou, H. Chen, Y. Hu, Z. Wang, S. Liu, W. Guo, X. Lu, Can N, S Cocoordination Promote Single Atom Catalyst Performance in $CO_2$RR? Fe-$N_2S_2$ Porphyrin versus Fe-$N_4$ Porphyrin, Small, 17 (2021) 2100949.

[125] Y. Zhao, J. Liang, C. Wang, J. Ma, G.G. Wallace, Tunable and Efficient Tin Modified Nitrogen-Doped Carbon Nanofibers for Electrochemical Reduction of Aqueous Carbon Dioxide, Advanced Energy Materials, 8 (2018) 1702524.
[126] A.A. Ensafi, H.A. Alinajafi, B. Rezaei, Pt-modified nitrogen doped reduced graphene oxide: A powerful electrocatalyst for direct $CO_2$ reduction to methanol, Journal of Electroanalytical Chemistry, 783 (2016) 82-89.
[127] Z. Geng, X. Kong, W. Chen, H. Su, Y. Liu, F. Cai, G. Wang, J. Zeng, Oxygen Vacancies in ZnO Nanosheets Enhance $CO_2$ Electrochemical Reduction to CO, Angewandte Chemie International Edition, 57 (2018) 6054-6059.
[128] J. Zhang, R. Yin, Q. Shao, T. Zhu, X. Huang, Oxygen Vacancies in Amorphous InOx Nanoribbons Enhance $CO_2$ Adsorption and Activation for $CO_2$ Electroreduction, Angewandte Chemie International Edition, 58 (2019) 5609-5613.
[129] B.H. Qin, Y.H. Li, H.J. Wang, G.X. Yang, Y.H. Cao, H. Yu, Q. Zhang, H. Liang, F. Peng, Efficient electrochemical reduction of $CO_2$ into CO promoted by sulfur vacancies, Nano Energy, 60 (2019) 43-51.
[130] Y.F. Wang, Z. Chen, P. Han, Y.H. Du, Z.X. Gu, X. Xu, G.F. Zheng, Single-Atomic Cu with Multiple Oxygen Vacancies on Ceria for Electrocatalytic $CO_2$ Reduction to $CH_4$, ACS Catalysis, 8 (2018) 7113-7119.
[131] S. Gao, Z. Sun, W. Liu, X. Jiao, X. Zu, Q. Hu, Y. Sun, T. Yao, W. Zhang, S. Wei, Y. Xie, Atomic layer confined vacancies for atomic-level insights into carbon dioxide electroreduction, Nature Communications, 8 (2017) 14503.
[132] P. Yang, Z.J. Zhao, X. Chang, R. Mu, S. Zha, G. Zhang, J. Gong, The Functionality of Surface Hydroxy Groups on the Selectivity and Activity of Carbon Dioxide Reduction over Cuprous Oxide in Aqueous Solutions, Angewandte Chemie International Edition, 57 (2018) 7724-7728.
[133] K. Lv, C. Teng, M. Shi, Y. Yuan, Y. Zhu, J. Wang, Z. Kong, X. Lu, Y. Zhu, Hydrophobic and Electronic Properties of the E-$MoS_2$ Nanosheets Induced by FAS for the $CO_2$ Electroreduction to Syngas with a Wide Range of $CO/H_2$ Ratios, Advanced Functional Materials, 28 (2018) 1802339.
[134] Y. Mun, S. Lee, A. Cho, S. Kim, J.W. Han, J. Lee, Cu-Pd alloy nanoparticles as highly selective catalysts for efficient electrochemical reduction of $CO_2$ to CO, Applied Catalysis B: Environmental, 246 (2019) 82-88.
[135] D. Kim, J. Resasco, Y. Yu, A.M. Asiri, P. Yang, Synergistic geometric and electronic effects for electrochemical reduction of carbon dioxide using gold-copper bimetallic nanoparticles, Nature Communications, 5 (2014) 4948.
[136] I. Bhugun, D. Lexa, J.M. Saveant, Catalysis of the electrochemical reduction of carbon dioxide by iron(0) porphyrins. Synergistic effect of Lewis acid cations, The Journal of Physical Chemistry, 100 (1996) 19981-19985.
[137] A. Schizodimou, G. Kyriacou, Acceleration of the reduction of carbon dioxide in the presence of multivalent cations, Electrochimica Acta, 78 (2012) 171-176.
[138] S. Kaneco, K. Iiba, H. Katsumata, T. Suzuki, K. Ohta, Effect of sodium cation on the electrochemical reduction of $CO_2$ at a copper electrode in methanol, Journal of Solid State Electrochemistry, 11 (2007) 490-495.
[139] S. Kaneco, K. Iiba, K. Ohta, T. Mizuno, Reduction of carbon dioxide to petrochemical intermediates, Energy Sources, 22 (2000) 127-135.
[140] B. Eneau-Innocent, D. Pasquier, F. Ropital, J.M. Leger, K.B. Kokoh, Electroreduction of carbon dioxide at a lead electrode in propylene carbonate: A spectroscopic study, Applied Catalysis B: Environmental, 98 (2010) 65-71.
[141] S. Ikeda, T. Takagi, K. Ito, Selective Formation of Formic-Acid, Oxalic-Acid, and Carbon-Monoxide by Electrochemical Reduction of Carbon-Dioxide, Bulletin of the Chemical Society of Japan, 60 (1987) 2517-2522.

[142] M. Asadi, K. Kim, C. Liu, A.V. Addepalli, P. Abbasi, P. Yasaei, P. Phillips, A. Behranginia, J.M. Cerrato, R. Haasch, P. Zapol, B. Kumar, R.F. Klie, J. Abiade, L.A. Curtiss, A. Salehi-Khojin, Nanostructured transition metal dichalcogenide electrocatalysts for $CO_2$ reduction in ionic liquid, Science, 353 (2016) 467-470.
[143] Y. Matsubara, D.C. Grills, Y. Kuwahara, Thermodynamic Aspects of Electrocatalytic $CO_2$ Reduction in Acetonitrile and with an Ionic Liquid as Solvent or Electrolyte, ACS Catalysis, 5 (2015) 6440-6452.
[144] E.E.L. Tanner, C. Batchelor-McAuley, R.G. Compton, Carbon Dioxide Reduction in Room-Temperature Ionic Liquids: The Effect of the Choice of Electrode Material, Cation, and Anion, The Journal of Physical Chemistry C, 120 (2016) 26442-26447.